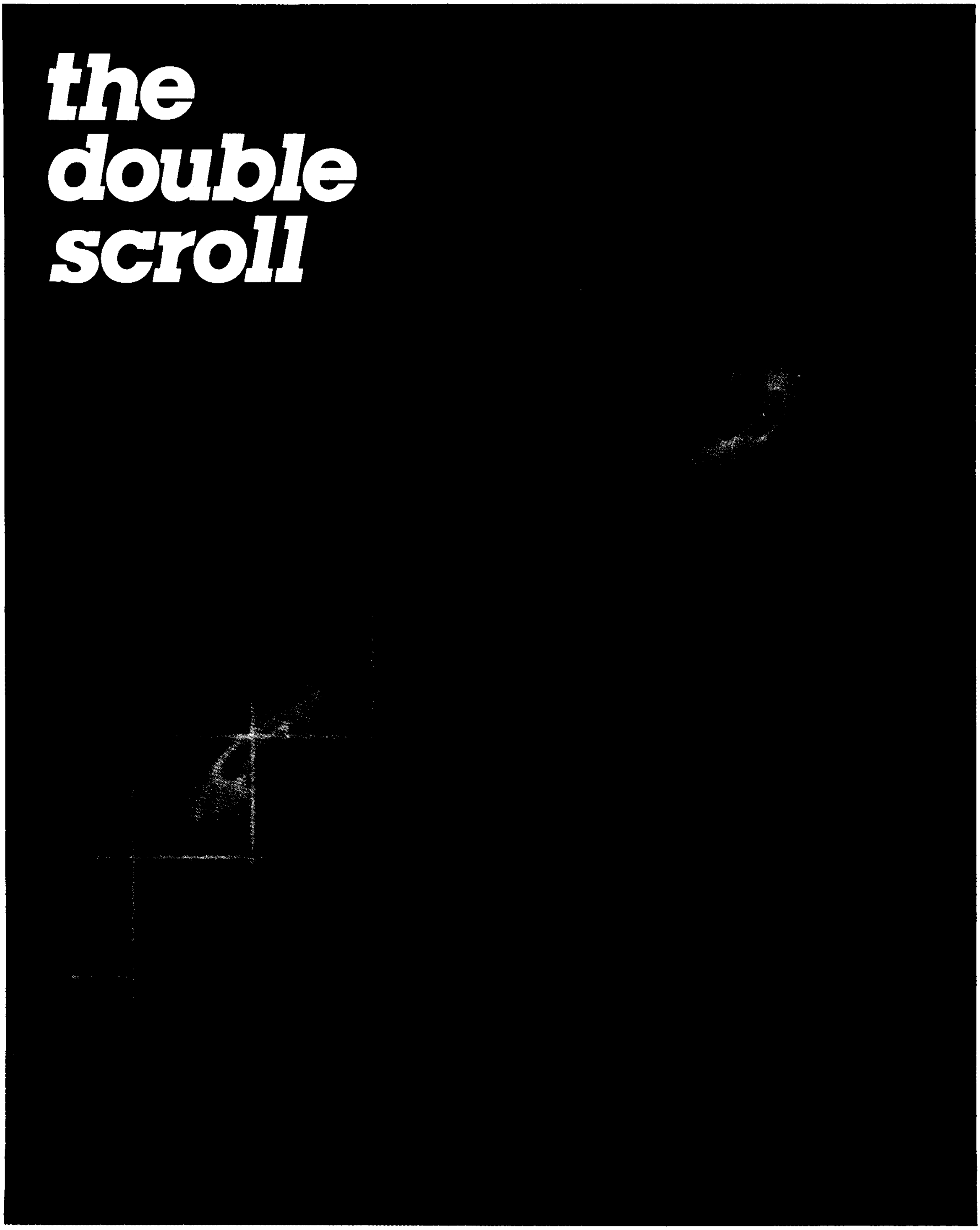
the
double
scroll

The Double Scroll

TAKASHI MATSUMOTO, FELLOW, IEEE, LEON O. CHUA, FELLOW, IEEE, AND MOTOMASA KOMURO

***Abstract*—A detailed analysis is given of the geometric structure of a chaotic attractor observed from an extremely simple autonomous electrical circuit. It is third order, reciprocal, and has only one nonlinear element: a 3-segment piecewise-linear resistor. Extensive laboratory measurements from this circuit and a detailed geometrical analysis and computer simulation reveal the following rather intricate "anatomy" of the associated *strange* attractor:**

In addition to a microscopically infinite sheet-like composition the attractor has a macroscopic *"double-scroll"* structure, i.e., two sheet-like objects are curled up together into spiral forms with infinitely many rotations. (See frontispiece.) The chaotic nature of this circuit is further confirmed by calculating its associated *Lyapunov exponents* and *Lyapunov dimension.* The double-scroll attractor has one *positive*, one zero and one negative Lyapunov exponent. The Lyapunov dimension turns out to be a *fractal* between 2 and 3 which agrees with the observed structures. The *power spectra* of the three associated state variables obtained by both measurement and computer simulation show a continuous broad spectrum typical of chaotic systems.

I. INTRODUCTION

THIS PAPER gives a detailed analysis of a chaotic attractor observed with an extremely simple autonomous electrical circuit which was reported earlier [1], [2].[1] The circuit is third order, reciprocal, and has only one nonlinear element, a *3-segment piecewise-linear resistor*.

Consider the circuit of Fig. 1(a) where the constitutive relation of the nonlinear resistor is given by Fig. 1(b). The circuit dynamics is described by

$$\boxed{\begin{aligned} C_1\frac{dv_{C_1}}{dt} &= G(v_{C_2}-v_{C_1})-g(v_{C_1})\\ C_2\frac{dv_{C_2}}{dt} &= G(v_{C_1}-v_{C_2})+i_L\\ L\frac{di_L}{dt} &= -v_{C_2}\end{aligned}} \quad (1.1)$$

where v_{C_1}, v_{C_2}, and i_L denote the voltage across C_1, the voltage across C_2 and the current through L, respectively,

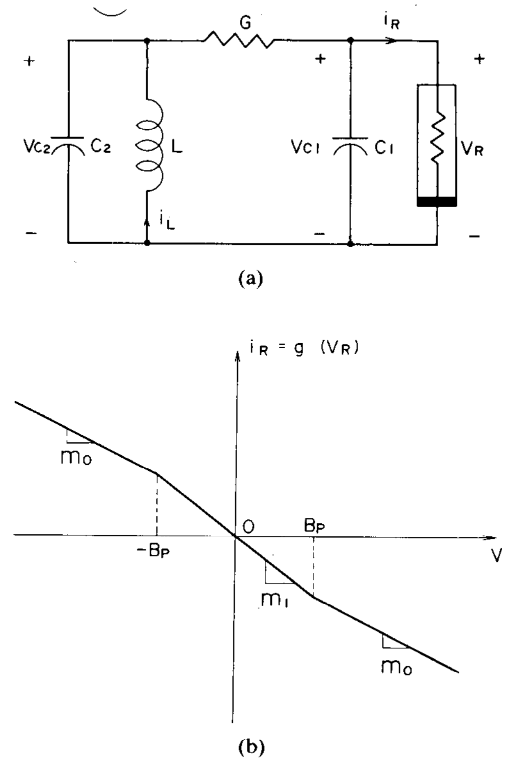

Fig. 1. A simple autonomous circuit with a chaotic attractor. (a) The circuitry. (b) Constitutive relation of the nonlinear resistor.

and $g(v_{C_1})$ is the piecewise-linear function in Fig. 1(b):[2]

$$g(v_{C_1}) = m_0 v_{C_1} + \tfrac{1}{2}(m_1-m_0)|v_{C_1}+B_p| + \tfrac{1}{2}(m_0-m_1)|v_{C_1}-B_p|. \quad (1.2)$$

Fig. 2 shows the chaotic attractor observed by solving (1.1) with

$$1/C_1 = 9, \quad 1/C_2 = 1, \quad 1/L = 7, \quad G = 0.7,$$
$$m_0 = -0.5, \quad m_1 = -0.8, \quad B_p = 1. \quad (1.3)$$

It is easy to realize (1.1) by a physical circuit. Fig. 3 shows the attractor with appropriate scaling seen by an oscilloscope. Fig. 4(a) gives the circuitry where the subcircuit within the broken-line box realizes the function $g(\cdot)$ of Fig. 1(b). The measured constitutive relation is given in Fig. 4(b). The component values indicated in Fig. 4(a) are

Manuscript received July 27, 1984; revised April 1, 1985. This work was supported in part by the Japanese Ministry of Education, the Saneyoshi Foundation, the Institute of Applied Electricity, the Science and Engineering Laboratory, the Tokutei-Kadai of Waseda University, by the Office of Naval Research under Contract N00014-70-C-0572, and by the National Science Foundation under Grant ECS-8542885.

T. Matsumoto is with the Department of Electrical Engineering, Waseda University, Tokyo 160, Japan.
L. O. Chua is with the Department of Electrical Engineering and Computer Sciences, University of California, Berkeley, CA 94720.
M. Komuro is with the Department of Mathematics, Tokyo Metropolitan University, Tokyo 158, Japan.

[1]The *double-scroll attractor* was first discovered in October 1983 and presented informally at a Special Session on Nonlinear Circuits at the *IEEE International Symposium on Circuits and Systems*, Montreal, May 1984.

[2]Our choice of a piecewise-linear function is for convenience in realization of the circuit as well as in analysis and programming. As will be seen in Section II, the piecewise-linearity simplifies the analysis in a significant manner. Any continuous piecewise-linear function has an explicit formula which requires only absolute value functions [3].

0098-4094/85/0800-0798$01.00 ©1985 IEEE

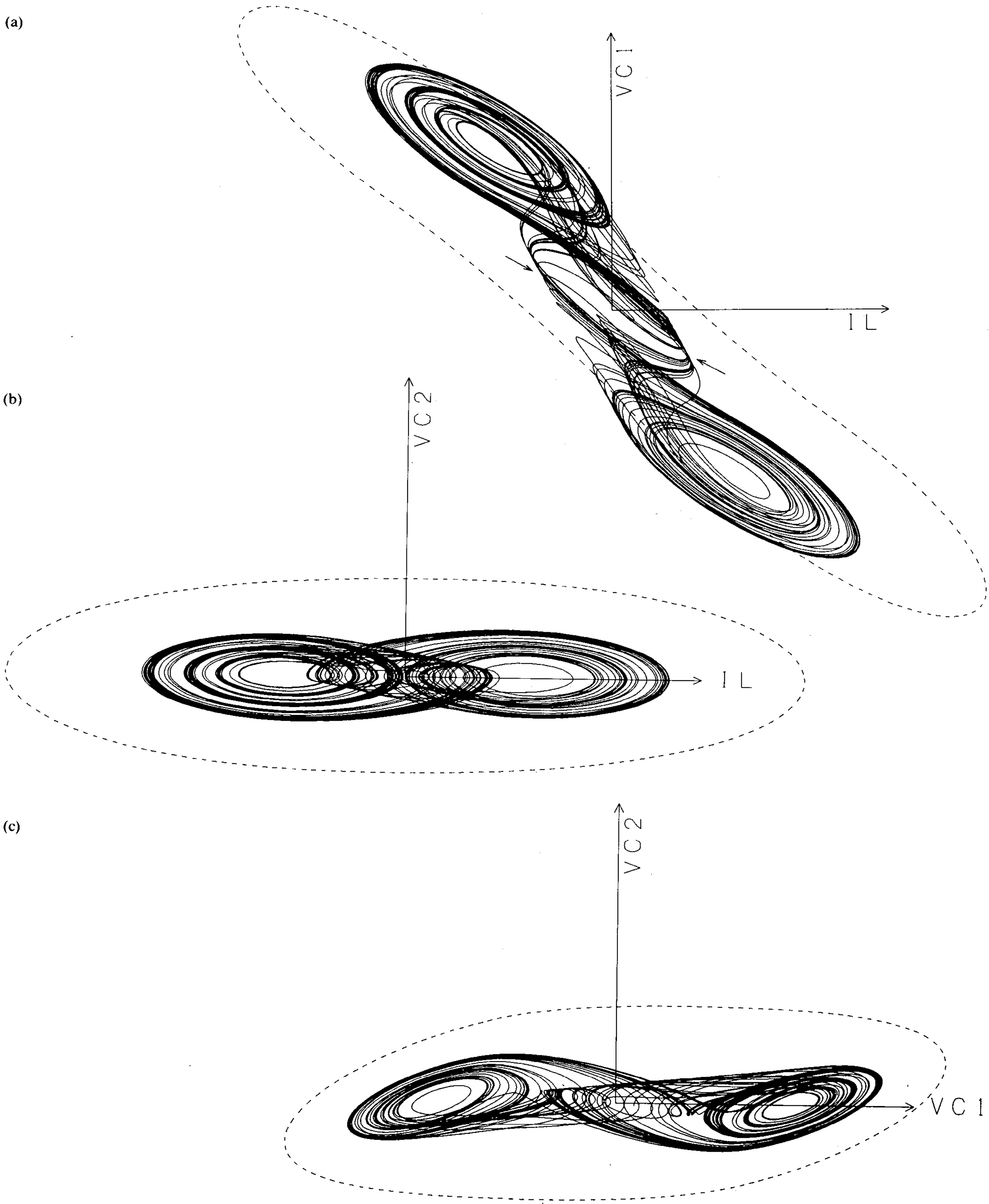

Fig. 2. The chaotic attractor and the saddle-type periodic orbit. (a) Projection onto the (i_L, v_{C_1})-plane. (b) Projection onto the (i_L, v_{C_2})-plane. (c) Projection onto the (v_{C_1}, v_{C_2})-plane. Runge–Kutta was iterated 10000 times with step size 0.04. Initial conditions: $v_{C_1}(0)=0.15264$, $v_{C_2}(0)=-0.02281$, $i_L(0)=0.38127$ for the attractor and $v_{C_1}(0)=2.532735$, $v_{C_2}(0)=1.285458\times10^{-3}$, $i_L(0)=-3.367482$ for the saddle-type periodic orbit with period 3.54793. The length of each arrow is 2.5.

"nominal" values of the components actually used in the measurement. Due to component tolerance, the actual values that would exactly duplicate the computer-simulated results could be within 15 percent of the nominal values. For example, the exact scaled component values needed to duplicate the results in Fig. 2 are as follows:

$$C_1 = 0.0055\ \mu\text{F}, \qquad C_2 = 0.0495\ \mu\text{F}$$
$$L = 7.07\ \text{mH}, \qquad R = 1.428\ \text{k}\Omega$$
$$m_0 = -0.5, \qquad m_1 = -0.8, \qquad \text{and } B_p = 1\ \text{V}.$$

The units of all voltage and current variables are measured in volts and milliamperes, respectively.

The usage of the word "chaotic attractor" is of course not rigorous in this paper as well as in other papers, in the sense that its existence has not been proven *mathematically*.[3] However, we have succeeded in providing a *physical* proof by designing and building a physical circuit whose *equation of motion* is modelled[4] by (1.1).

We cannot overemphasize that the circuit of Fig. 4 is *not* an analog computer in the sense that its building blocks are *not* integrators. They are ordinary circuit elements; namely, resistors, inductors and capacitors. Both current and voltage of each circuit element play a crucial role in the dynamics of the circuit. On the contrary, the variables in a typical analog computer are merely node voltages of the capacitor–integrator building-block modules where the circuit current is completely irrelevant in the circuit's dynamic operation. Hence it would be misleading to confuse our circuit as an analog computer. Indeed, any abstraction or generalization of the term "analog computer" on our circuit would imply that all physical circuits, or for that matter all physical systems, are analog computers, an implication which is absurd.

Equation (1.1) with the parameters specified in (1.3) has three equilibria: one at the origin, one at the "center" of the "upper hole", and one at the center of the "lower hole." A typical trajectory in the attractor rotates around one of the two outer equilibria, say the upper one, in a counterclockwise direction with respect to the left handed coordinate system. After each rotation the trajectory gets further from the equilibrium until a certain time after which there are two possibilities: (i) the trajectory goes back to a position closer to the equilibrium and repeats a similar process, (ii) the trajectory does not go back to a point close to the equilibrium but descends downward (with respect to the v_{C_1}-axis) in a spiral path and "lands" on the lower part of the attractor. The point where it lands is close to the lower equilibrium and starts rotating counterclockwise around the lower hole. After this, the behavior is similar to that in the upper part of the attractor except for the fact that it starts ascending after rotating around the lower equilibrium several times. The number of rotations a trajectory makes around an equilibrium *before* it starts descending or ascending is random—sometimes only twice and other times ten times. The number of rotations it makes *while* it descends or ascends is also random. Detailed reasoning for such behaviors will be given in Section II.

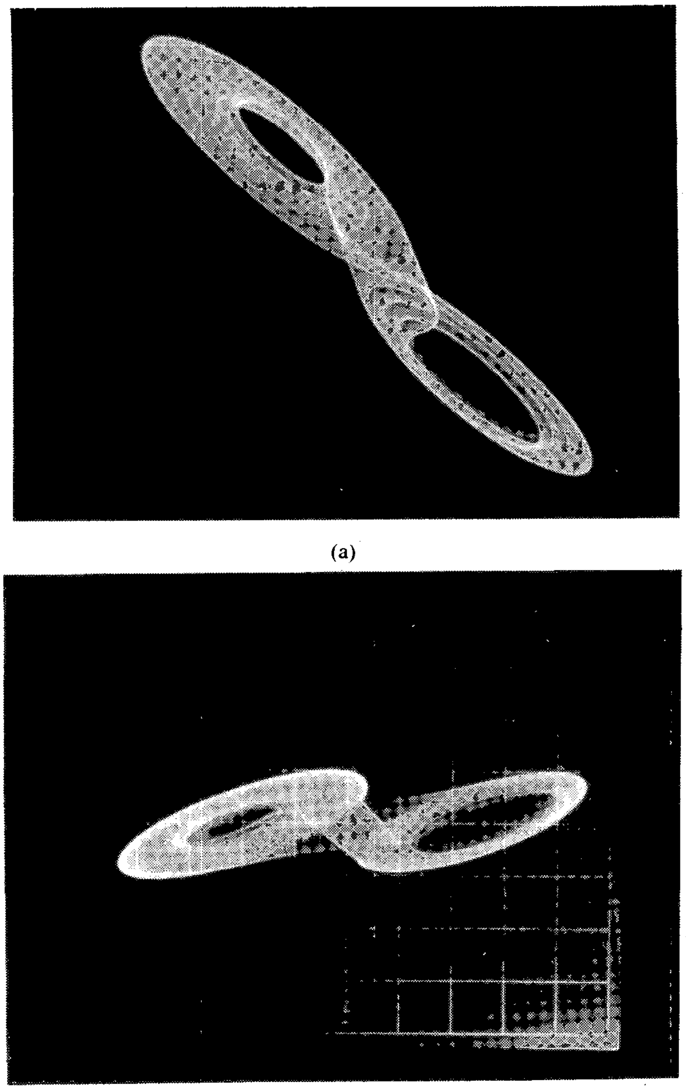

Fig. 3. The chaotic attractor observed by a circuit realization. (a) Projection onto the (i_L, v_{C_1})-plane. Horizontal Scale: 2 mA/division. Vertical scale: 2 V/division. (b) Projection onto the (v_{C_1}, v_{C_2})-plane. Horizontal scale: 2 V/division. Vertical scale: 2 V/division.

Let us pause to give a circuit-theoretic interpretation of the chaotic behavior. First note that the parallel connection (tank circuit) of C_2 and L constitutes a lossless oscillatory mechanism in the (v_{C_2}, i_L)-plane, whereas the conductance G provides the interactions between the (C_2, L)-oscillatory component and the active resistor $g(\cdot)$ together with C_1. This active resistor is of course responsible for the circuit's chaotic behavior. If this resistor were *locally passive* [11], it

[3] It has been argued by many researchers that "chaotic attractors" observed by digital simulation are of questionable validity because chaotic systems are by nature extremely sensitive to local truncation and round-off errors.

[4] Of course, due to component tolerances, the physical circuit in Fig. 4 is not exactly modelled by (1.1) with the parameters specified in (1.3). However, the fact that this circuit exhibits a chaotic attractor on an oscilloscope shows that (1.1) is indeed a robust model.

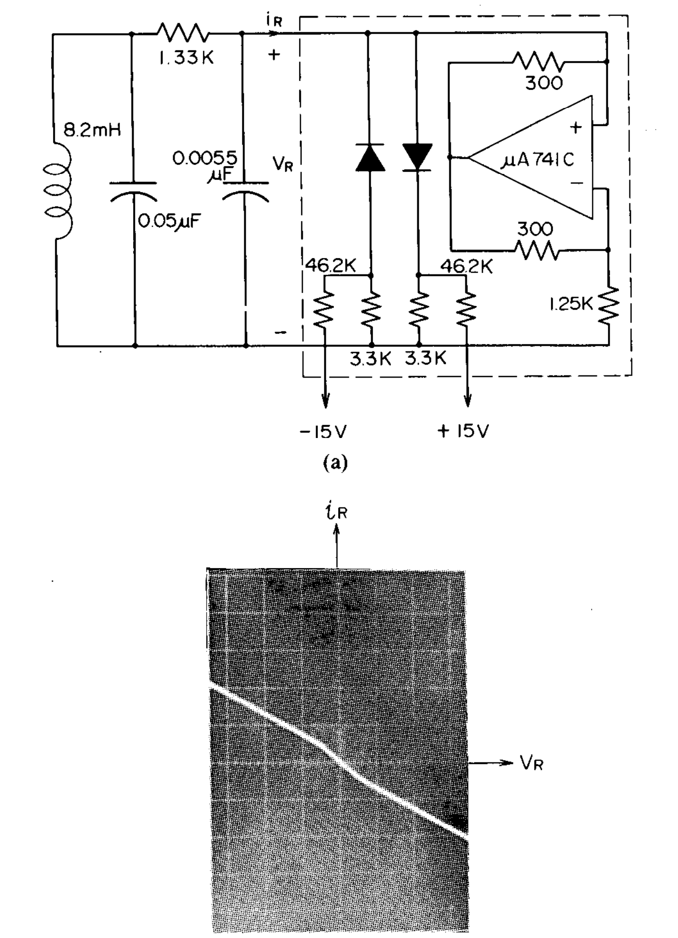

Fig. 4. Circuit realization. (a) The circuitry which realizes (1.1) with appropriate scaling: $C_1 = 0.0055\ \mu$F, $C_2 = 0.05\ \mu$F, $L = 8.2$ mH, and $R = 1.33$ kΩ. The box with broken lines realizes $g(\cdot)$ of Fig. 1(b). The volume of the resistors are: 46.2 kΩ, 3.3 kΩ, 300 Ω, and 1.25 kΩ. (b) Observed constitutive relation of $g(\cdot)$. Horizontal scale: 2 V/division. Vertical scale: 2 mA/division.

is well known that the circuit would be quite tame: all solutions would approach a globally asymptotically stable equilibrium. Since $g(\cdot)$ *is locally active* [11], i.e., $v_R(t)i_R(t) < 0$ (except at the origin) it keeps supplying power to the external circuit. The attracting nature of the chaotic trajectories is, therefore, due to the power dissipated in the *passive* element G, thereby restraining its growth.

Now, it is interesting to observe that there is a closed orbit (broken curve) outside the chaotic attractor. This orbit is *not* a stable limit cycle, however, since it cannot be observed in the oscilloscope from the physical circuit of Fig. 4(a) or obtained by ordinary numerical integration of (1.1). Neither is it a repelling periodic orbit since it cannot be observed by integrating (1.1) in backward time. It is, rather, *a saddle-type* [4] periodic orbit: its Poincaré map is stable in one direction but unstable in another direction. Newton iteration was used to find an initial point on this orbit via the "shooting method" [5, ch. 17].

If the more physically inclined reader feels uncomfortable with the function $g(\cdot)$ in Fig. 1(b) because it is not *eventually passive* [11] and there are initial conditions from

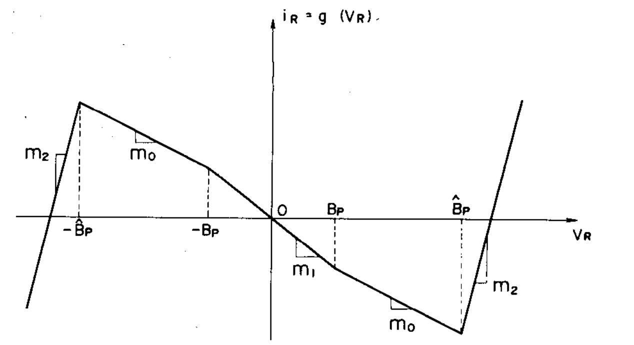

Fig. 5. A modified constitutive relation of the nonlinear resistor.

which the trajectories of (1.1) would diverge to infinity, he can simply replace Fig. 1(b) with Fig. 5. If $\hat{B}_P \geq 3$, the substituted characteristic curve has *no effect* on the attractor *and* on the saddle-type periodic orbit, because $|v_{C_1}(t)| < 3$ for all $t \geq 0$ on the attractor and on the saddle-type periodic orbit. The only difference is the additional appearance of a large *stable* limit cycle (periodic attractor) as shown in Fig. 6 ($\hat{B}_p = 3$, $m_2 = 5$), where (1.1) does not diverge with any initial condition.

In Fig. 6 there are three initial conditions:

(i)

$$v_{C_1}(0) = 0.15264$$
$$v_{C_2}(0) = -0.02281$$
$$i_L(0) = 0.38127$$

for the chaotic attractor,

(ii)

$$v_{C_1}(0) = 2.532735$$
$$v_{C_2}(0) = 1.285458 \times 10^{-3}$$
$$i_L(0) = -3.367482$$

for the saddle-type periodic orbit with period 3.54794, and

(iii)

$$v_{C_1}(0) = -3.08832$$
$$v_{C_2}(0) = -1.0423$$
$$i_L(0) = 6.93155$$

for the large periodic attractor with period 2.87.

Note that the saturation characteristic of the op amp naturally gives rise to eventual passivity for $g(\cdot)$. The saturation occurs, however, in regions too far away from the attractor for it to have any effect on the attractor. For readers interested in building our circuit with the prescribed parameters for the characteristic in Fig. 5, see [2].

The attractor appears to persist in a strong manner: the shape does not seem to change qualitatively with fairly large variations of parameters. It has been observed that the attractor persists for at least the following parameter ranges:

(i) $8.82 \leq 1/C_1 \leq 10.6$, when $1/C_2 = 1$, $1/L = 7$ and $G = 0.7$ are fixed,

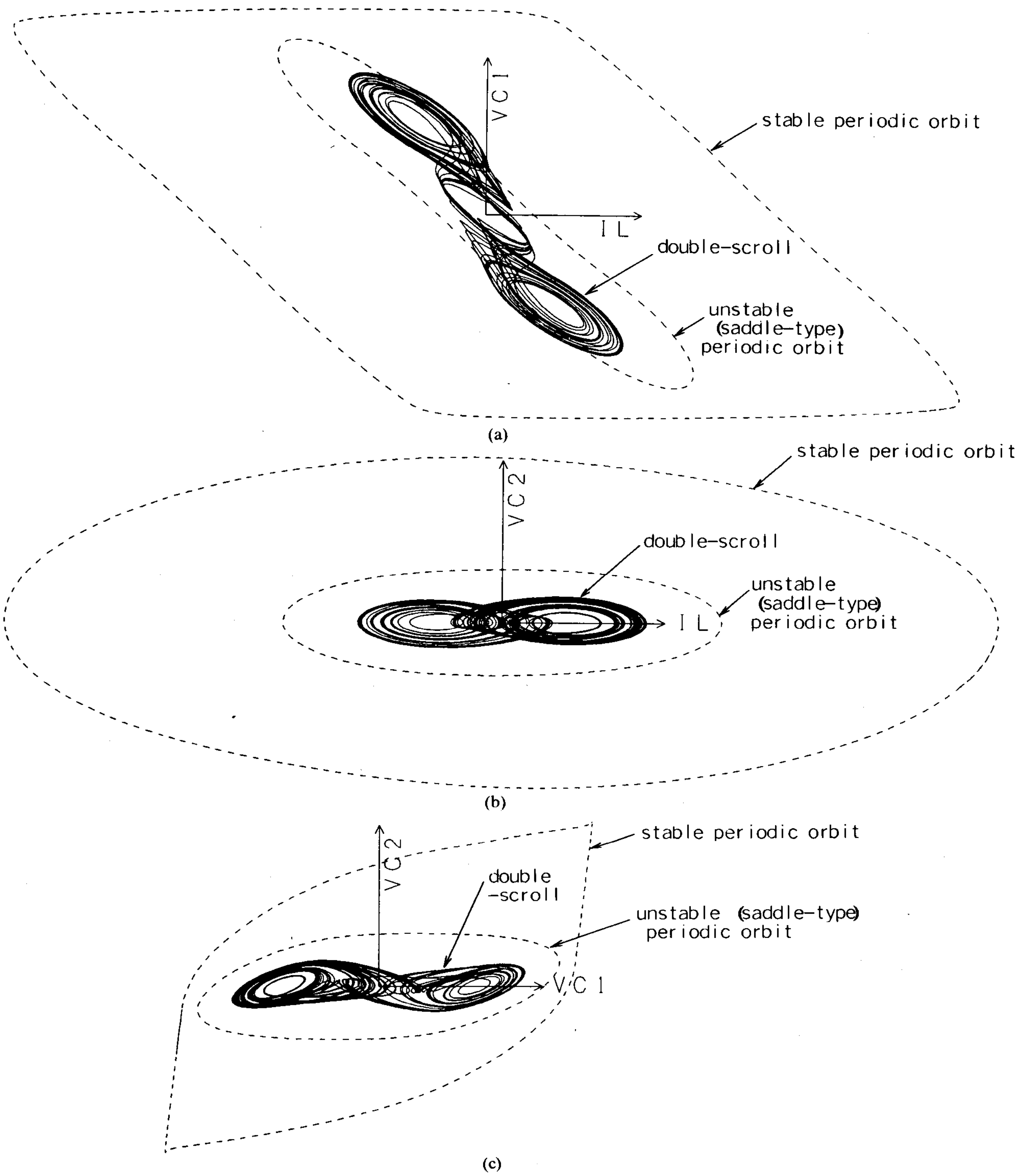

Fig. 6. The large stable limit cycle with the chaotic attractor and the saddle-type periodic orbit. (a) Projection onto the (i_L, v_{C_1})-plane. (b) Projection onto the (i_L, v_{C_2})-plane. (c) Projection onto the (v_{C_1}, v_{C_2})-plane. Initial conditions for the large stable limit cycle: $v_{C_1}(0) = -3.08832$, $v_{C_2}(0) = -1.0423$, $i_L(0) = 6.93155$ with period 2.87. The lenght of each arrow is 2.5.

(ii) $0.5 \leq 1/C_2 \leq 1.08$, when $1/C_1 = 9$, $1/L = 7$ and $G = 0.7$ are fixed,

(iii) $5.7 \leq 1/L \leq 7.13$, when $1/C_1 = 9$, $1/C_2 = 1$ and $G = 0.7$ are fixed, and

(iv) $0.68 \leq G \leq 0.76$, when $1/C_1 = 9$, $1/C_2 = 1$ and $1/L = 7$ are fixed.

Since there are two attractors in Fig. 6 (the chaotic attractor and the periodic attractor), one naturally wonders what boundary separates the domain of attraction for the chaotic attractor and the domain of attraction for the periodic attractor. Similarly, in Fig. 2, one wonders what distinguishes those initial states that are attracted to the

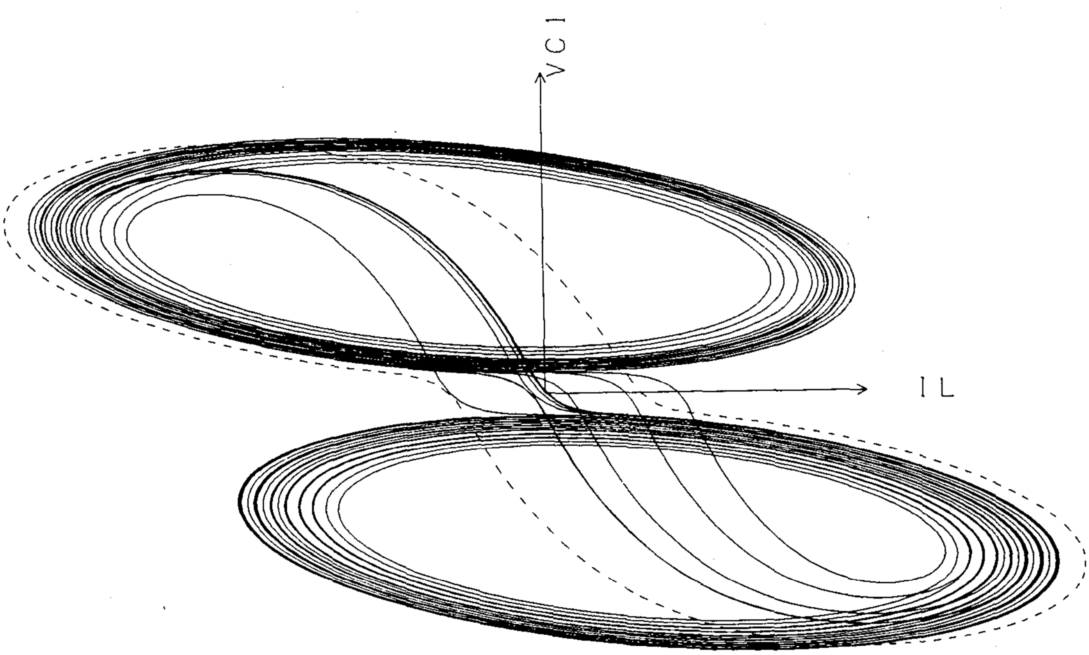

Fig. 7. The chaotic attractor and the saddle-type periodic orbit observed with the set of parameter values (1.4). Initial conditoins: $v_{C_1}(0) = 1.45305$, $v_{C_2}(0) = -4.36956$, $i_L(0) = 0.15034$ for the attractor, and $v_{C_1}(0) = 10.00717$, $v_{C_2}(0) = 1.80100$, $i_L(0) = -23.90375$ for the saddle-type periodic orbit with period 3.93165. The length of each arrow is 15.

chaotic attractor and those initial states from which (1.1) diverges. This is an interesting but difficult question. It appears that the stable manifold of the saddle-type periodic orbit decomposes $\mathbb{R}^3$ into two regions in a very complicated manner.

The set of parameter values given by (1.3) is different from the one reported in [1]; namely,

$$1/C_1 = 10, \quad 1/C_2 = 0.5, \quad 1/L = 7, \quad G = 0.7,$$
$$m_0 = -0.1, \quad m_1 = -4, \quad B_p = 1. \tag{1.4}$$

The equation for $g(v_{C_1})$ is given by (1.2).

The attractor observed with the set of parameter values in (1.4) is shown in Fig. 7. Of course, a large stable limit cycle is present in this case also if one replaces $g(\cdot)$ of Fig. 1(b) with Fig. 5 ($m_2 = 5$, $\hat{B}_p = 14$). Let us explain why we chose (1.3) instead of (1.4). In Fig. 7, a typical trajectory in the attractor behaves in a manner similar to that of Fig. 2(a) except that the "spiral staircase" is not clearly visible and that the trajectories which go back closer to the center of the hole without descending are indiscernible. When Fig. 7 was first observed [1], the following question naturally arose: "What object separates those trajectories which remain in the upper ring and those which move down to the lower ring?" If that object was detected, then an important part of the structure of the attractor would be understandable. We tried to find the "object" numerically by changing initial conditions. It was extremely sensitive to small changes in the initial conditions and we were unable to detect it. In order to see the reason note that the behavior of (1.1) is strongly influenced by the eigenvalues and the eigenspaces of its equilibria, which are well-defined concepts here since (1.1) is piecewise linear and since each region has a unique equilibrium. Note that (1.1) has three equilibria: one at the origin, one located approximately at the center of the upper hole, call it $\boldsymbol{P}^+$, and another located at a point symmetric with respect to the origin, call it $\boldsymbol{P}^-$. Each equilibrium has one real eigenvalue and two complex conjugate eigenvalues. At $\boldsymbol{P}^+$ (and $\boldsymbol{P}^-$) the real eigenvalue associated with (1.4) is

$$\gamma_p \approx -6.37$$

and the other two are

$$\sigma_p \pm j\omega_p \approx 0.01 \pm j1.82.$$

At the origin, the eigenvalues are

$$\gamma_0 \approx 33.07$$
$$\sigma_0 \pm j\omega_0 \approx -0.21 \pm j1.86.$$

It is clear that γ_0, the real eigenvalue at the origin, completely overwhelms the others, i.e., the rate of expansion at the origin is extremely strong and a digital computer (a finite *discrete* machine) is unable to show clearly the structure of the *continuous* flow generated by (1.1) with (1.4).

With (1.3), the eigenvalues are

$$\gamma_p \approx -2.76$$
$$\sigma_p \pm j\omega_p \approx 0.13 \pm j2.13$$
$$\gamma_0 \approx 1.55$$
$$\sigma_0 \pm j\omega_0 \approx -0.68 \pm j1.90.$$

All of them are within a compatible range and the elusive

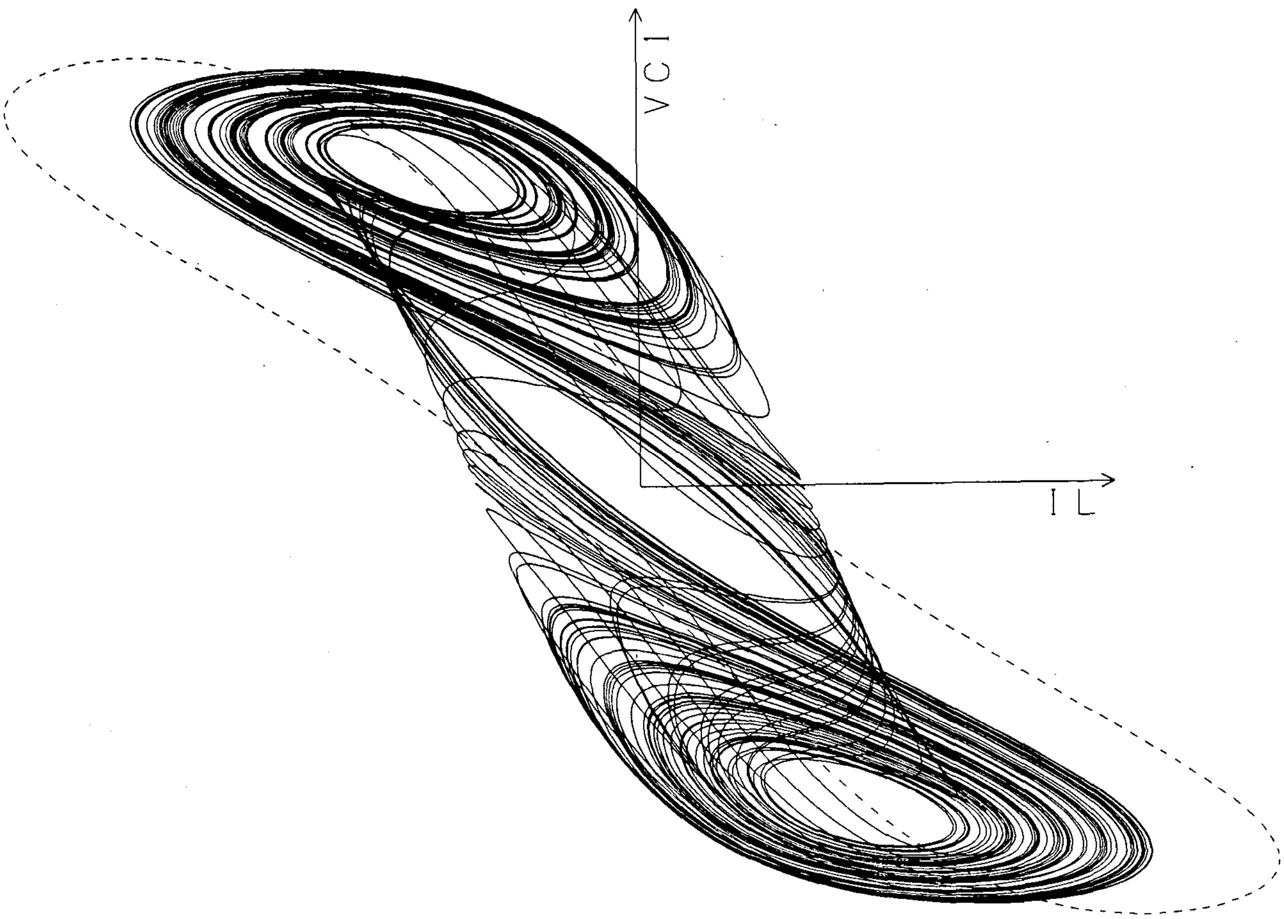

Fig. 8. The chaotic attractor and the saddle-type periodic orbit with the smooth resistor constitutive relation (1.5). Initial conditions: $v_{C_1}(0) = 1.47147$, $v_{C_2}(0) = 0.83242$, $i_L(0) = 2.23418$ for the attractor, and $v_{C_1}(0) = 9.998048$, $v_{C_2}(0) = 1.980972$, $i_L(0) = -10.908448$ for the saddle-type periodic orbit with period 4.49. The length of each arrow is 11.

object[5] that we were looking for turned out to be the *stable eigenspace [6] of the origin*. Moreover, an interesting structure different from Lorenz's [7] and Rössler's [8] has been observed as will be described in the next section.

Finally, note that the function $g(\cdot)$ of Fig. 1(b) does not have to be piecewise-linear to observe qualitatively the same attractor. Let us replace, for example, $g(\cdot)$ of Fig. 1(b) with the smooth cubic function

$$g(v_{C_1}) = a_0 v_{C_1}\left(\frac{a_1^2}{3}v_{C_1}^2 - 1\right) \tag{1.5}$$

where $a_0 = 0.8$, $a_1 = 0.1$. Then with $1/C_1 = 9$, $1/C_2 = 0.5$, $1/L = 7$, $G = 0.65$, the qualitatively similar chaotic attractor of Fig. 8 has been observed.

In Section II we will give a detailed description of the geometric structure of the attractor. In Section III, we will give our computation of the *Lyapunov exponents* which give important quantitative information associated with an attractor, and then calculate the *Lyapunov dimension*. It turns out to be a *fractal* between 2 and 3. Finally, in Section IV, we will give the power spectra of the time waveforms $v_{C_1}(t)$, $v_{C_2}(t)$, and $i_L(t)$ associated with those state variables.

[5] To be precise, the object we are trying to identify must separate all orbits *belonging to the attractor* into those which remain in the upper region from those which descend down to the lower region.

II. Geometric Structure of the Attractor

2.1. Preliminary Observations

Recall the dynamics (1.1) and note that the function $g(\cdot)$ of Fig. 1(b) is given by

$$g(v_R) \triangleq g(v_R;\, B_p, m_0, m_1)$$

$$= \begin{cases} m_0 v_R + B_p(m_1 - m_0), & v_R \geq B_p \\ m_1 v_R, & |v_R| \leq B_p \\ m_0 v_R - B_p(m_1 - m_0), & v_R \leq -B_p. \end{cases} \tag{2.1}$$

This function satisfies

$$g(B_p v_R;\, B_p, m_0, m_1) = B_p g(v_R;\, 1, m_0, m_1). \tag{2.2}$$

Therefore, via the rescaling,

$$x \triangleq v_{C_1}/B_p, \quad y \triangleq v_{C_2}/B_p, \quad z \triangleq i_L/(B_p G),$$
$$\tau \triangleq tG/C_2, \quad a \triangleq m_1/G, \quad b \triangleq m_0/G,$$
$$\alpha \triangleq C_2/C_1, \quad \beta \triangleq C_2/(LG^2), \tag{2.3}$$

equation (1.1) is transformed into the following simpler dimensionless form:

$$\boxed{\begin{aligned} \frac{dx}{d\tau} &= \alpha(y - x - f(x)) \\ \frac{dy}{d\tau} &= x - y + z \\ \frac{dz}{d\tau} &= -\beta y \end{aligned}} \tag{2.4}$$

where

$$f(x) \triangleq g(x; 1, b, a) = \begin{cases} bx + a - b, & x \geq 1 \\ ax, & |x| \leq 1 \\ bx - a + b, & x \leq -1. \end{cases} \tag{2.5}$$

Equation (2.4) is dynamically equivalent to (1.1) but is more convenient since some of the parameters are normalized. Our analysis below will be based on (2.4). This dimensionless equation will also be convenient when we investigate various bifurcations in later papers.

We begin with the following observations:

(i) Equation (2.4) is symmetric with respect to the origin, i.e., the vector field is invariant under the transformation

$$(x, y, z) \to (-x, -y, -z). \tag{2.6}$$

(ii) Consider the equilibria:

$$\begin{cases} x + f(x) = 0 \\ y = 0 \\ x + z = 0. \end{cases} \tag{2.7}$$

It follows from the form of $f(\cdot)$ that (2.4) has a unique equilibrium in each of the following three subsets of $\mathbb{R}^3$:

$$\begin{cases} D_1 \triangleq \{(x, y, z) | x \geq 1\} \\ D_0 \triangleq \{(x, y, z) | |x| \leq 1\} \\ D_{-1} \triangleq \{(x, y, z) | x \leq -1\} \end{cases} \tag{2.8}$$

provided that $a, b \neq -1$. The equilibria are explicitly given by

$$\begin{cases} \boldsymbol{P}^+ = (\ \ k, 0, -k) \in D_1 \\ \boldsymbol{0} \ \ = (\ \ 0, 0, \ \ 0) \in D_0 \\ \boldsymbol{P}^- = (-k, 0, \ \ k) \in D_{-1} \end{cases} \tag{2.9}$$

where $k = (b - a)/(b + 1)$.

(iii) In each of D_1, D_0, and D_{-1}, (2.4) is linear. In fact, letting

$$\boldsymbol{x} \triangleq (x, y, z), \qquad \boldsymbol{k} \triangleq (k, 0, -k) \tag{2.10}$$

and introducing the 3×3 real matrix

$$\boldsymbol{A}(\alpha, \beta, c) \triangleq \begin{pmatrix} -\alpha(c+1) & \alpha & 0 \\ 1 & -1 & 1 \\ 0 & -\beta & 0 \end{pmatrix} \tag{2.11}$$

where $\boldsymbol{A}$ depends on α, β (see (2.3)) and a parameter c, which is equal to a in D_0, and b in D_1 and D_{-1}, we can recast (2.4) as follows:

$$\boxed{\frac{d\boldsymbol{x}}{dt} = \begin{cases} \boldsymbol{A}(\alpha, \beta, b)(\boldsymbol{x} - \boldsymbol{k}), & \boldsymbol{x} \in D_1 \\ \boldsymbol{A}(\alpha, \beta, a)\boldsymbol{x}, & \boldsymbol{x} \in D_0 \\ \boldsymbol{A}(\alpha, \beta, b)(\boldsymbol{x} + \boldsymbol{k}), & \boldsymbol{x} \in D_{-1} \end{cases}} \tag{2.12}$$

Here, we have abused our notation for *time*: it should have been τ instead of t (see (2.3)). There will be no confusion, however. The set of parameter values (α, β, a, b) corresponding to (1.3) is given (via (2.3)) by

$$(\alpha, \beta, a, b) = (9, 14\tfrac{2}{7}, -\tfrac{8}{7}, -\tfrac{5}{7}).$$

Then the matrix

$$\boldsymbol{A}_p \triangleq \boldsymbol{A}(9, 14\tfrac{2}{7}, -\tfrac{5}{7})$$

associated with the regions D_1 and D_{-1} has a real eigenvalue

$$\gamma_p \approx -3.94$$

and a pair of complex-conjugate eigenvalues

$$\sigma_p \pm j\omega_p \approx 0.19 \pm j3.05.$$

Similarly, the matrix

$$\boldsymbol{A}_0 \triangleq \boldsymbol{A}(9, 14\tfrac{2}{7}, -\tfrac{8}{7})$$

associated with the region D_0 has a real eigenvalue

$$\gamma_0 \approx 2.22$$

and a pair of complex-conjugate eigenvalues

$$\sigma_0 \pm j\omega_0 \approx -0.97 \pm j2.71.$$

Note that the relative sizes of eigenvalues remain unchanged even after rescaling via (2.3). Let $E^s(\boldsymbol{P}^\pm)$ be the eigenspace corresponding to the real eigenvalue γ_p at $\boldsymbol{P}^\pm$ and let $E^u(\boldsymbol{P}^\pm)$ be the eigenspace[6] corresponding to the complex eigenvalues $\sigma_p \pm j\omega_p$ at $\boldsymbol{P}^\pm$. Similarly, let $E^u(\boldsymbol{0})$ and $E^s(\boldsymbol{0})$ be the eigenspaces corresponding to γ_0 and $\sigma_0 \pm j\omega_0$, respectively. Then,

$$\dim E^s(\boldsymbol{P}^\pm) = \dim E^u(\boldsymbol{0}) = 1$$
$$\dim E^u(\boldsymbol{P}^\pm) = \dim E^s(\boldsymbol{0}) = 2$$

and the eigenspaces are given explicitly by the following

[6] Throughout this paper, we use the same terminology "eigenspace" to denote the vector space spanned by the real and imaginary parts of the complex-conjugate eigenvectors.

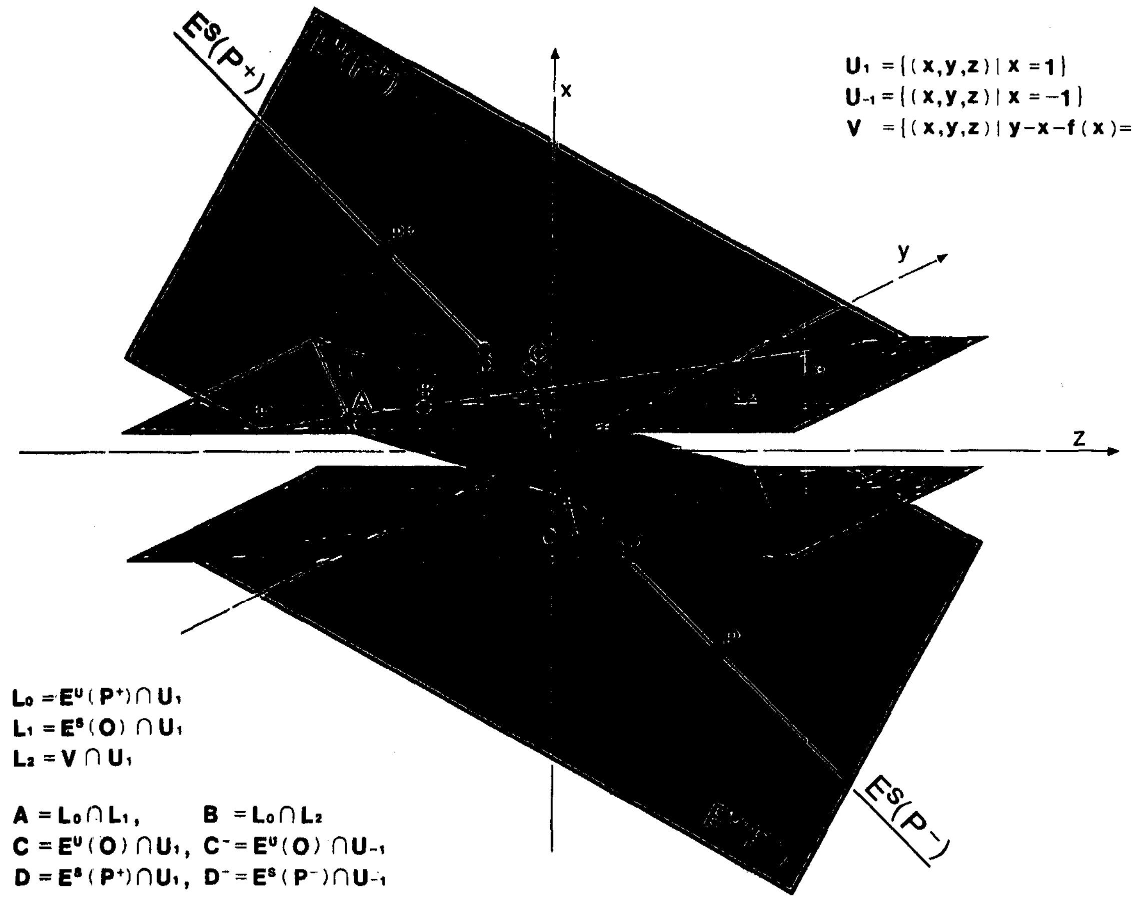

Fig. 9. Eigenspaces of the equilibria and related sets.

equations:

$$E^s(\boldsymbol{P}^\pm):\quad \frac{x\mp k}{\gamma_p^2+\gamma_p+\beta}=\frac{y}{\gamma_p}=\frac{z\pm k}{-\beta}$$

$$E^u(\boldsymbol{P}^\pm):\quad (\gamma_p^2+\gamma_p+\beta)(x\mp k)+\alpha\gamma_p y + \alpha(z\pm k)=0$$

$$E^u(\boldsymbol{0}):\quad \frac{x}{\gamma_0^2+\gamma_0+\beta}=\frac{y}{\gamma_0}=\frac{z}{-\beta}$$

$$E^s(\boldsymbol{0}):\quad (\gamma_0^2+\gamma_0+\beta)x+\alpha\gamma_0 y+\alpha z=0.$$

2.2. The Geometric Structure

Now we turn to describe the structure of the attractor. Define (see Fig. 9)

$$U_1 \triangleq D_1\cap D_0=\{(x,y,z)|x=1\}$$

$$U_{-1} \triangleq D_{-1}\cap D_0=\{(x,y,z)|x=-1\}$$

$$V \triangleq \{(x,y,z)|\dot{x}=0\} = \{(x,y,z)|y-x-f(x)=0\}$$

$$L_0 \triangleq E^u(\boldsymbol{P}^+)\cap U_1$$

$$L_1 \triangleq E^s(\boldsymbol{0})\cap U_1$$

$$L_2 \triangleq V\cap U_1$$

$$A \triangleq L_0\cap L_1,\quad B\triangleq L_0\cap L_2$$

$$C \triangleq E^u(\boldsymbol{0})\cap U_1,\quad C^-\triangleq E^u(\boldsymbol{0})\cap U_{-1}$$

$$D \triangleq E^s(\boldsymbol{P}^+)\cap U_1,\quad D^-\triangleq E^s(\boldsymbol{P}^-)\cap U_{-1}.$$

$F \triangleq$ a point on L_0 to the left of and sufficiently far from A.

Note that U_1, U_{-1}, and V are 2-dimensional objects, L_0, L_1 and L_2 are lines while A, B, C, C^-, D, D^-, and F are points.

Let φ^t be the flow generated by (2.4) and pick an initial condition $x_0\in E^u(\boldsymbol{P}^+)$ in a neighborhood of $\boldsymbol{P}^+$. Then, for $t>0$, the flow $\varphi^t(x_0)$ starts wandering away from $\boldsymbol{P}^+$ *on* $E^u(\boldsymbol{P}^+)$. After winding round $\boldsymbol{P}^+$ several times in a *counterclockwise* direction,[7] it hits the plane U_1 at some

[7]To show the direction is counterclockwise, pick any point P_0 (on the eigenspace $E^u(\boldsymbol{P}^+)$) whose y-coordinate is positive. Equation (2.4) then implies that $dz/dt<0$ (since $\beta>0$) for the trajectory (passing through P_0) in a neighborhood of P_0. When this trajectory gets into the region whose y-coordinate is negative, then $dz/dt>0$.

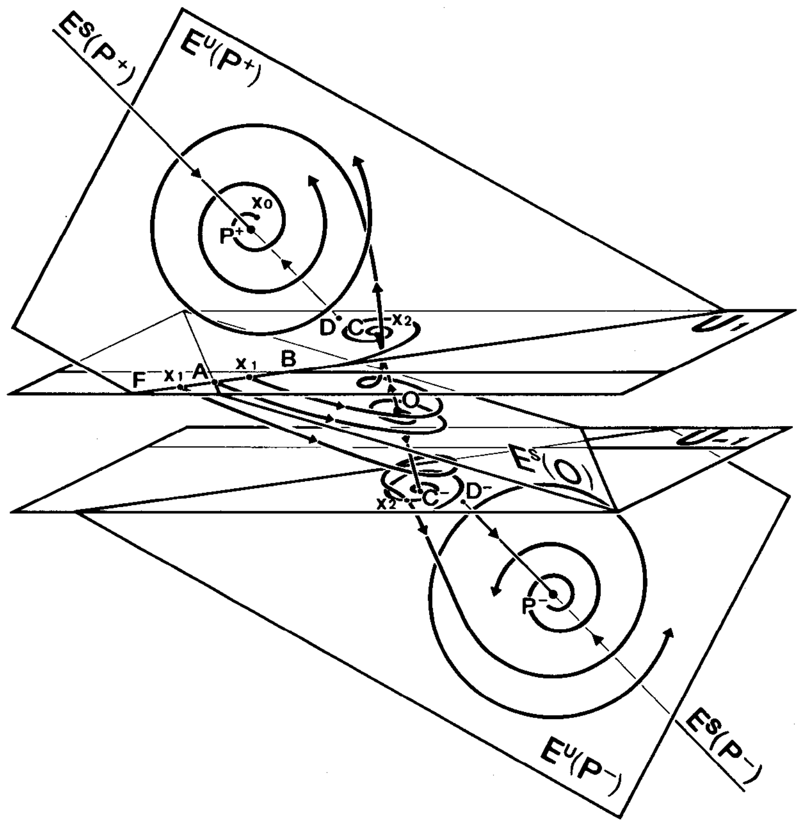

Fig. 10. Sketch of typical trajectories in the attractor.

time, say t_1: $x_1 \triangleq \varphi^{t_1}(x_0)$. The trajectory up to t_1 is a spiral since (2.4) is linear in D_1 and since $E^u(P^+)$ is invariant. Clearly $x_1 \in L_0$. Note that the line L_2 is a straight line parallel to the z-axis because $\dot{x}$ is independent of z. Observe that L_2 separates the plane U_1 into two regions, one (to which A belongs) where $\dot{x} < 0$ and another where $\dot{x} > 0$. Since $\varphi^t(x_0)$ hits the plane U_1 downward (recall that the motion is counterclockwise) at $t = t_1$, one sees that x_1 belongs to the line segment $\overline{FB}$, i.e., $\dot{x} < 0$ at x_1. The "fate" of $\varphi^t(x_1)$ depends crucially on which part of $\overline{FB}$ x_1 lies (see Fig. 10).

Case 1: $x_1 = A$

Since the dynamics is linear in D_0, one can check analytically that $\varphi^t(A)$ never hits U_{-1} directly for the parameter values (1.3), i.e., the real part σ_0 of the complex conjugate eigenvalues is negative and small enough compared to the imaginary part ω_0. (We will omit the details). Since $A \in E^s(\mathbf{0})$ and since $E^s(\mathbf{0})$ is invariant, $\varphi^t(x_1)$ approaches the origin asymptotically as $t \to \infty$ (see Fig. 10). The trajectory is a spiral with infinitely many rotations because (2.4) is linear in D_0 and $E^s(\mathbf{0})$ is invariant.

Case 2: $x_1 \in$ *Interior* $\overline{AB}$

In this case $\varphi^t(x_1)$ has two components in the sense that its projection onto $E^s(\mathbf{0})$ approaches the origin asymptotically and its projection onto $\overline{\mathbf{0}C} \subset E^u(\mathbf{0})$ wanders away from the origin. This means that $\varphi^t(x_1)$ moves up along a spiral with central axis $\overline{\mathbf{0}C}$ and then eventually hits U_1 again from below: $x_2 \triangleq \varphi^{t_2}(x_1)$. The number of rotations of $\varphi^t(x_1)$ around $\overline{\mathbf{0}C}$ can get arbitrarily large without bound if x_1 is very close to A. These processes naturally give rise to the map

$$\psi: \overline{AB} \to U_1$$

defined by

$$\psi(x_1) = x_2.$$

The image $\psi(\overline{AB})$ is a *spiral* with center at C which is tangent to L_0 at B. After hitting U_1, the trajectory $\varphi^t(x_2)$ has two components in the sense described above: one which stays in $E^u(P^+)$ and moves away from P^+ in a spiral manner and another in $E^s(P^+)$ which approaches P^+ asymptotically. Therefore, $\varphi^t(x_2)$ ascends in a spiral path with central axis $\overline{DP}^+$ and *flattens itself onto* $E^u(P^+)$ *from below* (see Fig. 10).

Case 3: $x_1 \in$ *Interior* $\overline{FA}$

$\varphi^t(x_1)$ has two components in the same sense as above. One component stays in $E^s(\mathbf{0})$ and asymptotically approaches $\mathbf{0}$ in a spiral manner. Another component stays in $E^u(\mathbf{0})$ and moves away from $\mathbf{0}$ on $\overline{\mathbf{0}C}^-$. This means that $\varphi^t(x_1)$ descends along a spiral with central axis $\overline{\mathbf{0}C}^-$, hits U_{-1} at $x_2 \triangleq \varphi^{t_2}(x_1)$ and enters the region D_{-1} eventually. The closer x_1 to the point A, the larger the number of rotations of $\varphi^t(x_1)$ around $\overline{\mathbf{0}C}^-$. After entering into D_{-1}, the flow $\varphi^t(x_2)$ consists of two components: one which is in $E^u(P^-)$ and moves away from P^- and another which stays in $E^s(P^-)$ and asymptotically approaches P^-. Therefore, $\varphi^t(x_2)$ descends spirally with the central axis

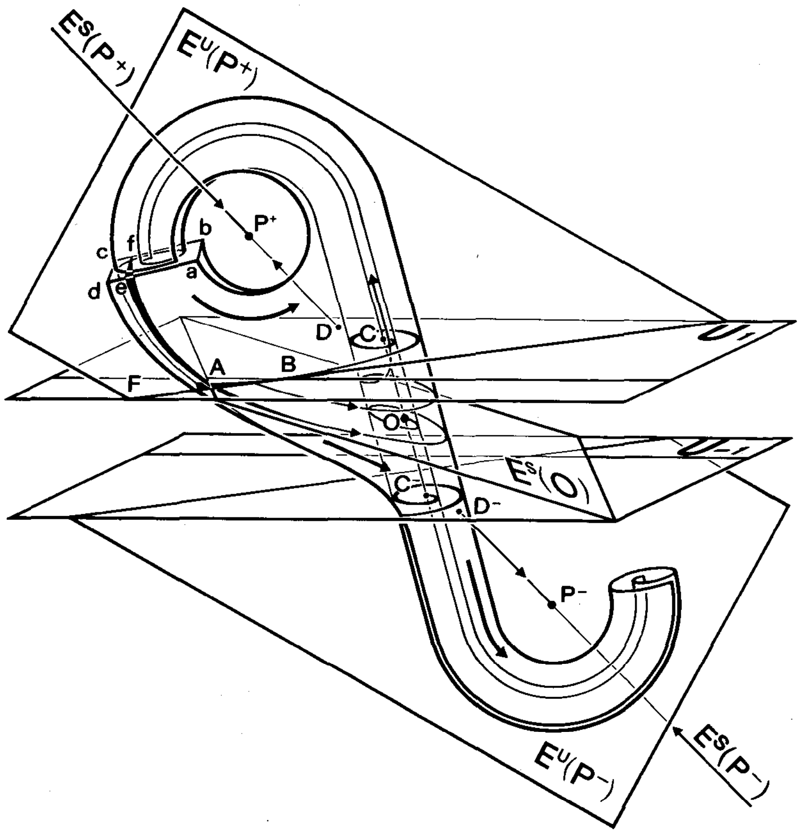

Fig. 11. Deformations of a rectangle which flows along the trajectories originating from points on the rectangle *abcd*.

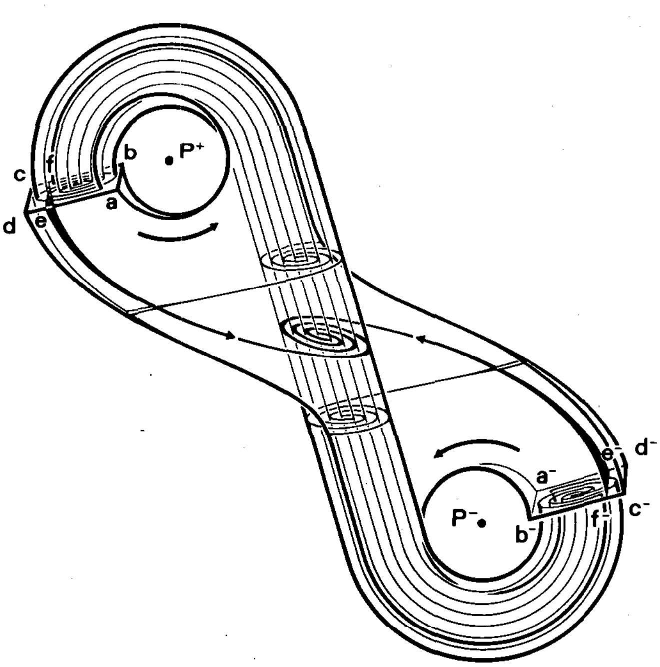

Fig. 12. Geometric structure of the double-scroll attractor.

$\overline{D^-P^-}$ and eventually *flattens itself onto* $E^u(P^-)$ *from above* (see Fig. 10).

In order to grasp the whole picture, pick a rectangle *abcd* in D_1 in such a way that $\overline{ad}$ is on $E^u(P^+)$ and $\overline{bc}$ lies below $E^u(P^+)$, i.e., on the side to which D belongs. Fig. 11 shows how the rectangle *abcd* changes its shape while flowing along φ^t. Suppose that the rectangle is thin enough and that it is chosen appropriately in such a way that the trajectories starting on the line segment $\overline{ef}$ hit L_1. Then, after hitting L_1, they approach the origin asymptotically in a spiral manner with infinitely many rotations. Trajectories starting in the rectangle *abfe* stay within D_1 or return to D_1 eventually even if they once spend some time in D_0. Trajectories with initial states in the rectangle *cdef* leave D_1, enter D_0, hit U_{-1} and enter D_{-1}. They turn around P^- and flatten themselves onto $E^u(P^-)$ from above.

Since (2.4) is symmetric with respect to the origin, one sees that a similar argument applies to a rectangle $a^-b^-c^-d^-$ in region U_{-1} located symmetrically with respect to the origin. Assembling all the information, one obtains a whole picture (Fig. 12). Observe that the rectangle *abcd* is mapped into two spiral regions with infinitely many rotations: *abfe* is mapped into one spiral region and *cdef* into another spiral region. Note that $E^s(\mathbf{0})$ plays an important role in determining the fate of a trajectory after hitting U_1 or U_{-1}. It differentiates those trajectories which descend (resp. ascend) from those which remain in the upper part (resp., lower part). This is barely discernible in Fig. 2(a) if one takes a careful look at it. There are two thin gaps (identified by arrows) between the sets of trajectories and $E^s(\mathbf{0})$ is sitting in these gaps.

Microscopically speaking, the two thin "rings" of the double-scroll attractor are made of infinitely many layers of points compressed into a thin sheet (think of infinitely many sheets of "lead" being hammered into one con-

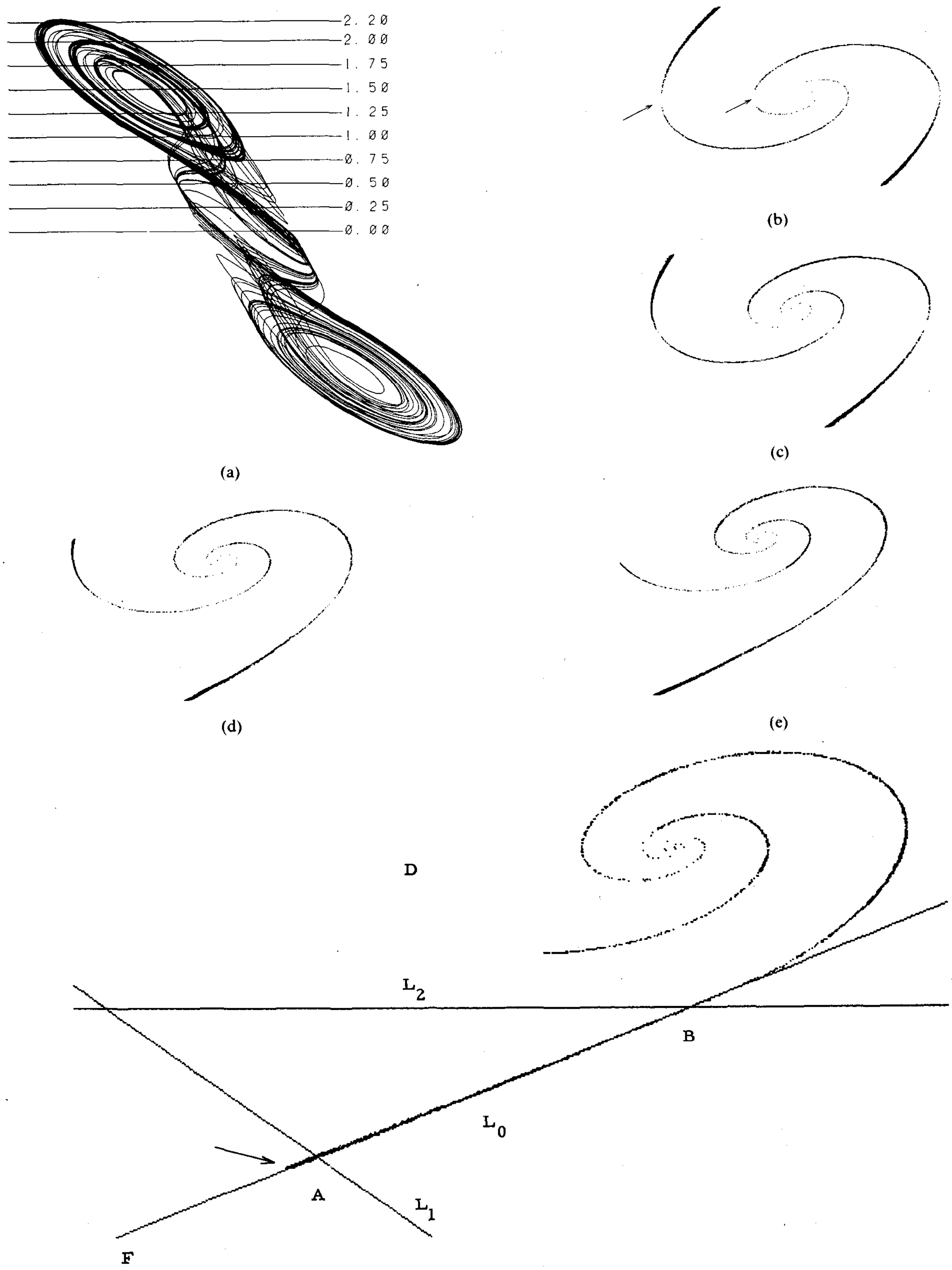

Fig. 13. Cross sections of the double-scroll attractor. (a) Locations of cross sections. (b) Cross section at $v_{C_1} = 0.00$. Arrows indicate the thin gaps where $E^s(\mathbf{0})$ is located. (c) Cross section at $v_{C_1} = 0.25$. (d) Cross section at $v_{C_1} = 0.50$. (e) Cross section at $v_{C_1} = 0.75$. (f) Cross section at $v_{C_1} = 1.00$ with related sets. The arrow indicates the "tail" of the attractor. (g) Cross section at $v_{C_1} = 1.25$. (h) Cross section at $v_{C_1} = 1.50$. (i) Cross section at $v_{C_1} = 1.75$. (j) Cross section at $v_{C_1} = 2.00$. (k) Cross section at $v_{C_1} = 2.20$. All of them have the same scaling.

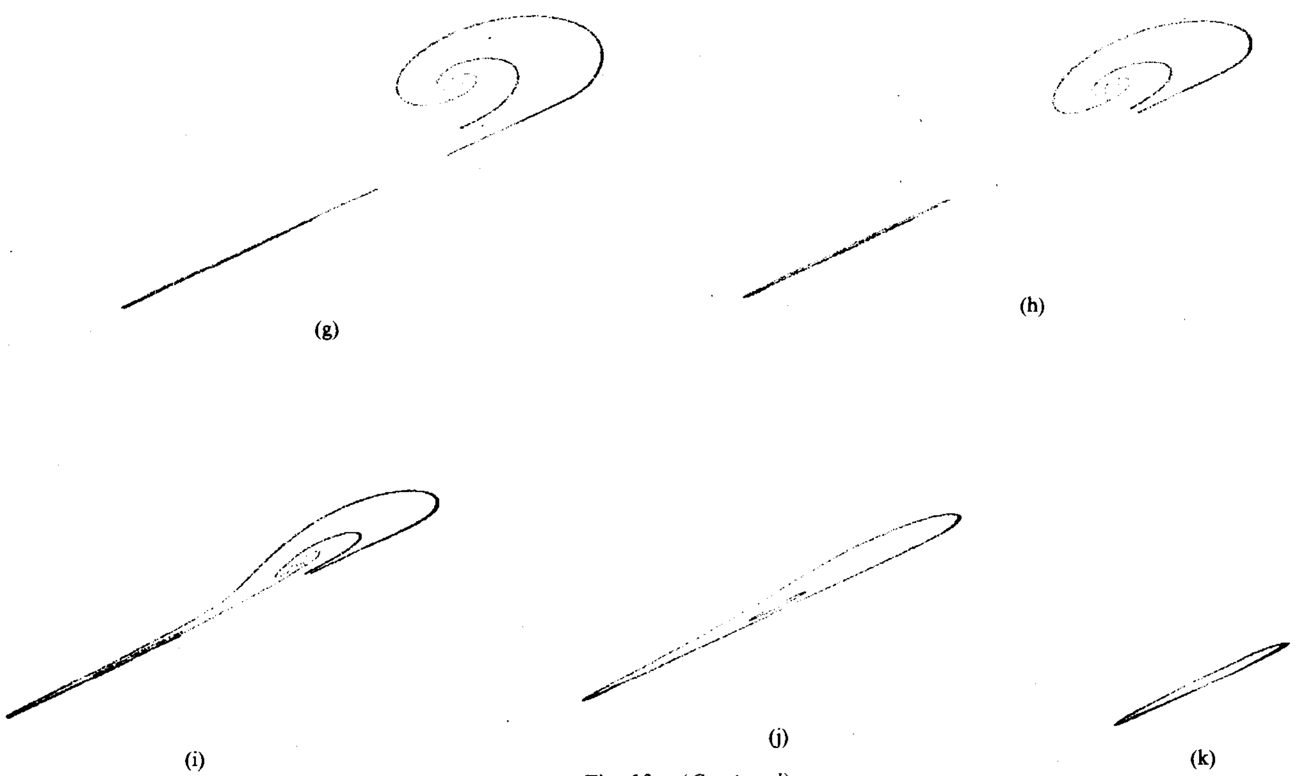

Fig. 13. (*Continued*)

glomerate sheet). *Macroscopically*, a good way of describing the "anatomy" of the above attractor would be a "*double-scroll*" structure since two sheet-like objects are curled up together into spiral forms with infinitely many rotations-while maintaining some space between the two scrolls which gradually decreases, thus causing them to meet eventually at some limit point.[8] In order to see the structure more clearly let us look at the cross sections of the attractor. Fig. 13(b)–(k) show cross sections of the attractor taken at

$$U(r) \triangleq \{(x, y, z) | x = r\}, \qquad r = 0.25k, \ k = 0, 1, \cdots, 8$$

and at $U(2.20)$. (The cross section at $U(2.25)$ is extremely small.) Fig. 13(a) shows positions of the cross sections. On the cross section at $U(1.00)$, various line segments and points related to Figs. 9–12 are superimposed. One can clearly observe the double-scroll structure and how the scrolls flatten themselves gradually. The cross section at $U(1.75)$ (Fig. 13(i)) is particularly interesting. The sheet-like structure is clearly discernible: it is folded many times. Moreover, one can observe that the flattening of the left portion is sharper than that of the right portion so that the spirals still survive on the right portion while they flatten themselves on the left portion. This stems from the fact that trajectories rotate around $\boldsymbol{P}^+$ in a *counterclockwise* direction and hence they flatten onto $E^u(\boldsymbol{P}^+)$ as time goes. Note that theoretically, the two scrolls are curled up infinitely many times even though numerical results reveal only several of them. One can also observe how $E^s(\mathbf{0})$ cuts the attractor. In Fig. 13(b), (c), and (d), there are small gaps in the spirals. (In Fig. 13(b) the gap is identified by arrows.) Since $E^s(\mathbf{0})$ is sitting in the gaps, the trajectories cannot get there (as long as numerical computations go). Those gaps correspond to the gaps in Fig. 2(a) as explained earlier. Fig. 14 is an abstract picture showing only the highlights of the main features of our attractor after several simplifications.

Now it is clear that the double-scroll attractor has a structure quite different from the well-known Lorenz [7] and the Rössler [8] attractors since the double-scroll structure has not been observed with the latter attractors. Recall that the Lorenz equation (at the popular parameter values $\sigma = 10$, $\beta = 8/3$, $\rho = 28$) has three equilibria: one at the origin, one in the half space $x > 0$ and another in the half space $x < 0$. Note that the origin belongs to the Lorenz attractor and that the same is true in our attractor. At the origin in the Lorenz attractor, however, all eigenvalues are real, whereas in our case the origin has one positive real eigenvalue and a pair of complex-conjugate eigenvalues. Recall also that the Lorenz equation is symmetric with respect to the z-axis while (1.1) is symmetric with respect to the origin. As for the Rössler equation [8], recall that it has only two equilibria. Furthermore, the attractor does not contain any equilibrium.

One of the reviewers for [1] pointed out that Sparrow [9] and Brockett [10] had observed chaotic attractors in feedback systems with 3-segment piecewise-linear feedback characteristics. Their equations also have three equilibria. The one reported in [9] does not appear to have the double-scroll structure. It does not seem to contain any equilibrium point. Furthermore, the equilibrium point in

[8]The microscopic features are akin to the "cells" whereas the macroscopic features are akin to the "organs."

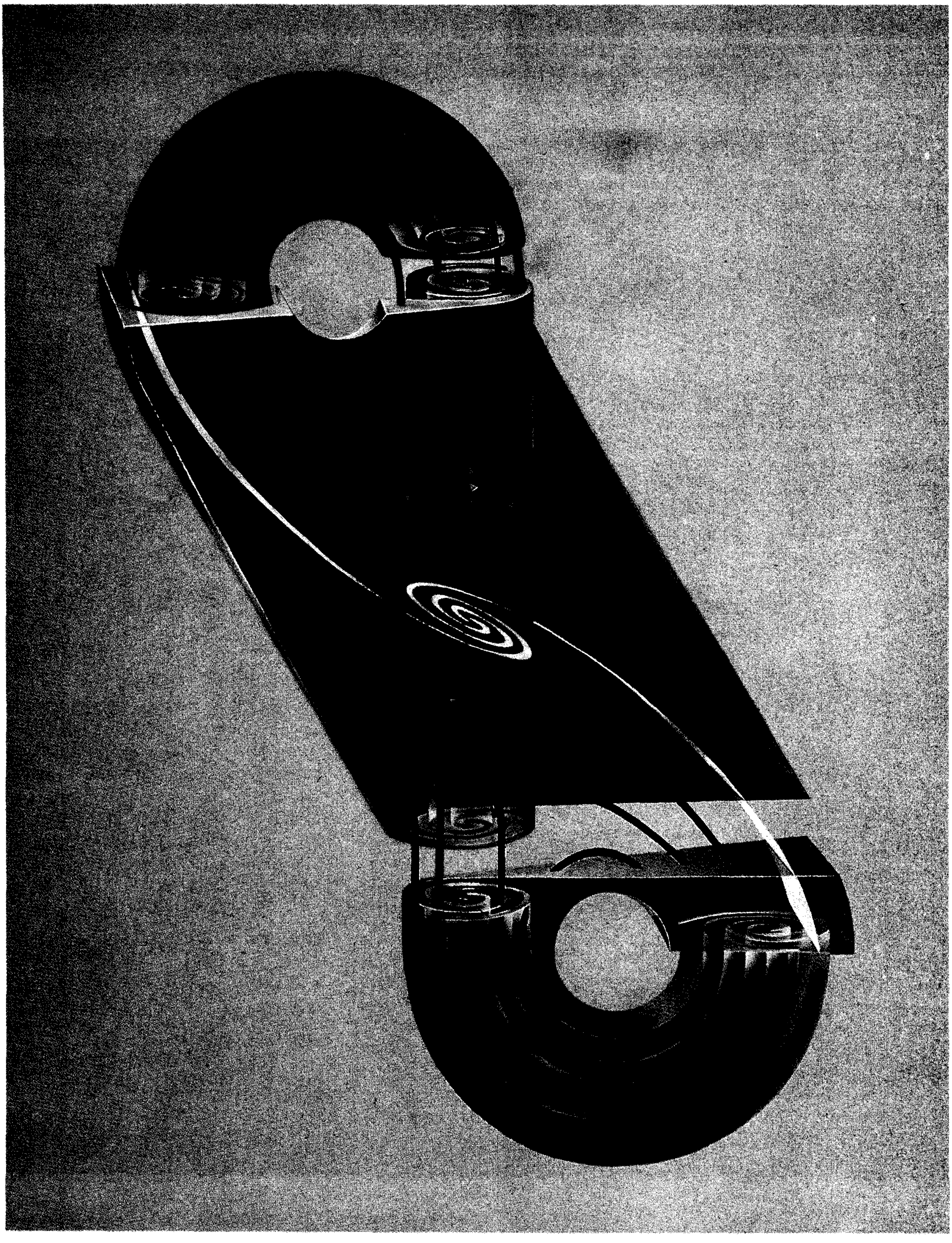

Fig. 14. An abstract geometric model of the double-scroll attractor which highlights only the key features.

the middle has one *negative* real eigenvalue and a pair of complex conjugate eigenvalues with *positive* real part, a combination which is different from ours.

Equilibria with the same stability types as in [9] can be realized in our circuit, by exchanging the slopes m_0 and m_1 of Fig. 1(b). Indeed, at $m_0 = -0.8$ and $m_1 = -0.5$, we have observed chaotic attractors similar to that of [9] when the other parameters are appropriately chosen. These chaotic attractors, however, readily lost their stability as we varied various parameters. One reason for this lack of robustness is that, in this case,

$$\dim E^s(\boldsymbol{P}^{\pm}) = \dim E^u(\mathbf{0}) = 2$$

$$\dim E^u(\boldsymbol{P}^{\pm}) = \dim E^s(\mathbf{0}) = 1.$$

Consequently, once a trajectory gets into the "wrong side" of $E^s(\boldsymbol{P}^{\pm})$, it diverges to infinity.[9]

The dynamics reported in [10] has the same type of equilibria as ours. It is not clear, however, whether it also exhibits the double-scroll structure described above.

Note also that the circuit of Fig. 1 has no coupling elements and is, therefore, *reciprocal* [11], while the systems in [7]–[10] do not appear to be realizable by reciprocal circuits. Moreover our equation appears to be the only one which accurately models a *real physical* system where experimental measurements agree remarkably well with computer simulations.

III. Lyapunov Exponents and Lyapunov Dimension

3.1. Lyapunov Exponents

First let us rewrite (1.1) as

$$\frac{dx}{dt} = \boldsymbol{F}(\boldsymbol{x}) \tag{3.1}$$

where $\boldsymbol{x} = (v_{C_1}, v_{C_2}, i_L)$ and let $\boldsymbol{\varphi}^t(\boldsymbol{x}_0)$ be its flow with initial condition $\boldsymbol{x}_0$. (We abused the notation $\boldsymbol{x}$. There will be no confusion, however.) Lyapunov exponents are generalizations of the *characteristic exponents* (defined only for periodic orbits) so that they make sense for the more general nonperiodic orbits. If Λ is a periodic orbit with period T and if $\boldsymbol{x}_0 \in \Lambda$, then the eigenvalues of $(\boldsymbol{D\varphi}^T)_{\boldsymbol{x}_0}$, denoted by e^{λ_1}, e^{λ_2}, and e^{λ_3}, are called the characteristic multipliers for Λ. The numbers λ_1, λ_2, and λ_3 are called the characteristic exponents. They give the rate of expansion and contraction of vectors in the tangent space $T_{x_0}\mathbb{R}^3$ along Λ. Since Λ is a closed curve, at least one of the three numbers, say e^{λ_1}, must be 1, and hence $\ln e^{\lambda_1} = 0$. If, in addition, $\ln e^{\lambda_2}, \ln e^{\lambda_3} < 0$, then Λ will be a periodic attractor, i.e., a stable limit cycle (Fig. 15(a)). If $\ln e^{\lambda_2} < 0$ and $\ln e^{\lambda_3} > 0$, then Λ will be a saddle-type periodic orbit (Fig. 15(b)). Now let Λ be a non-periodic invariant set, e.g., a chaotic attractor. There is a technical difficulty in defining characteristic multipliers for Λ. Recall that for a closed

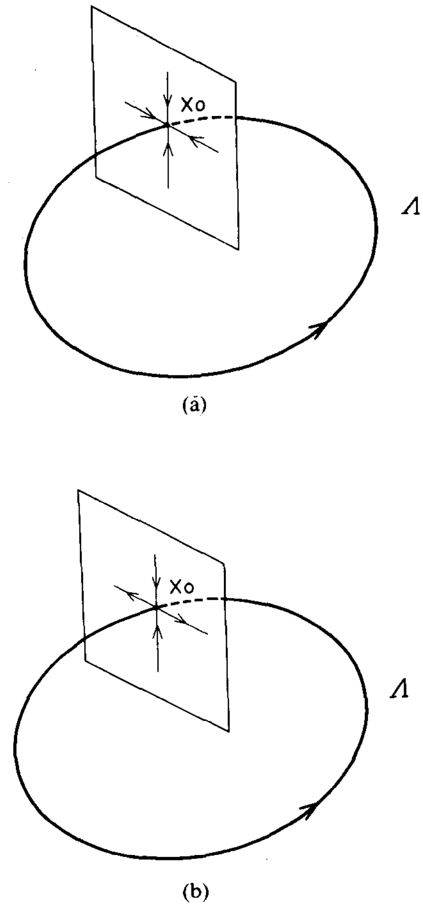

Fig. 15. Characteristic exponents for periodic orbits. (a) Stable limit cycle. (b) Saddle-type periodic orbit.

orbit, the eigenvalues of $(\boldsymbol{D\varphi}^T)_{x_0}$ are well defined since $(\boldsymbol{D\varphi}^T)_{x_0}$ maps $T_{x_0}\mathbb{R}^3$ into *itself*. On the other hand, this definition is not valid for Λ if it is nonperiodic since $(\boldsymbol{D\varphi}^t)_{x_0}$ does not necessarily map $T_{x_0}\mathbb{R}^3$ into itself for any t. The definition of Lyapunov exponents requires the invariance of the tangent subbundles. Suppose that for all $t > 0$, there are linear subspaces $E^1_{\varphi^t(x_0)} \supseteq E^2_{\varphi^t(x_0)} \supseteq E^3_{\varphi^t(x_0)}$ in $T_{\varphi^t(x_0)}\mathbb{R}^3$ and numbers $\mu_1(\boldsymbol{x}_0) \geq \mu_2(\boldsymbol{x}_0) \geq \mu_3(\boldsymbol{x}_0)$ such that

(i)

$$(\boldsymbol{D\varphi}^t)_{x_0} E^k_{x_0} = E^k_{\varphi^t(x_0)} \tag{3.2}$$

(ii)

$$\dim E^k_{\varphi^t(x_0)} = 4 - k \tag{3.3}$$

(iii)

$$\mu_k(\boldsymbol{x}_0) = \lim_{T \to \infty} \frac{1}{T} \ln \frac{\|(\boldsymbol{D\varphi}^T)_{x_0} \boldsymbol{e}\|}{\|\boldsymbol{e}\|},$$

$$\text{for all} \quad \boldsymbol{e} \in E^k_{x_0} - E^{k+1}_{x_0}, \; k = 1, 2, 3.$$

The numbers $\mu_1(\boldsymbol{x}_0)$, $\mu_2(\boldsymbol{x}_0)$, and $\mu_3(\boldsymbol{x}_0)$ are called the *Lyapunov exponents* for Λ if $\boldsymbol{x}_0 \in \Lambda$. They give the *average linearized expansion* and *contraction rates* of nearby points along an orbit. Note that $E^1_{x_0} - E^2_{x_0}$ consists of vectors in $T_{x_0}\mathbb{R}^3$ which expand at the fastest rate, $E^2_{x_0} - E^3_{x_0}$ consists

[9]We thank one of the reviewers for suggesting this observation which we had observed prior to writing this manuscript, but we did not feel this observation is of sufficient interest to warrant its inclusion.

of vectors which expand at the next fastest rate, and the vectors in $E^3_{x_0}$ expand at the slowest rate. In many cases the vectors in $E^3_{x_0}$ are contracted if Λ is an attractor.

The conditions under which Lyapunov exponents exist are strong [12] and are hard to check. Here we will only give our numerical results. They give, however, good quantitative information about the attractor described in the previous sections. The computations are non trivial since *one does not know* the invariant splittings $E^k_{\varphi^t(x_0)}$, $k=1,2,3$. One can, however, compute $\mu_1(x_0)$, the *largest exponent*, numerically, provided that $\mu_1(x_0)$, $\mu_2(x_0)$, and $\mu_3(x_0)$ are not too close to each other. In order to explain this, let $x_0 \in \Lambda$ and pick *any* $e \in T_{x_0}\mathbb{R}^3$. Then

$$\frac{1}{T}\ln\frac{\|(D\varphi^T)_{x_0}e\|}{\|e\|} \tag{3.4}$$

would give $\mu_1(x_0)$ for T large, because the subspace with the fastest expansion rate would eventually dominate the others and the vector $(D\varphi^T)_{x_0}e$ would fall in $E^1_{\varphi^T(x_0)} - E^2_{\varphi^T(x_0)}$ for any $e \in T_{x_0}\mathbb{R}^3$, T large.

Computations of $\mu_2(x_0)$ and $\mu_3(x_0)$ need some more care since $(D\varphi^T)_{x_0}e$ is dominated by $E^1_{\varphi^T(x_0)} - E^2_{\varphi^T(x_0)}$ and one does not know how to compute $E^2_{\varphi^T(x_0)} - E^3_{\varphi^T(x_0)}$. In order to overcome this problem, we compute

$$\mu_1(x_0)+\mu_2(x_0) \tag{3.5}$$

instead of $\mu_2(x_0)$. First note that the number (3.5) gives the average expansion or contraction rate of an *area element* of $E^1_{x_0} - E^3_{x_0}$. Let e_1 and e_2 span $E^1_{x_0} - E^3_{x_0}$. Then the exterior product $e_1 \wedge e_2$ is the parallelepiped generated by e_1 and e_2 [13]. Therefore,

$$\frac{1}{T}\ln\frac{\|(D\varphi^T)_{x_0}e_1 \wedge (D\varphi^T)_{x_0}e_2\|}{\|e_1 \wedge e_2\|} \tag{3.6}$$

would give (3.5) for T large. A numerical difficulty arises since $(D\varphi^T)_{x_0}e_1$ and $(D\varphi^T)_{x_0}e_2$ would eventually belong to or become very close to $E^1_{\varphi^T(x_0)} - E^2_{\varphi^T(x_0)}$ for the reason explained before. Hence the angle between $(D\varphi^T)_{x_0}e_1$ and $(D\varphi^T)_{x_0}e_2$ gets smaller and smaller, and numerical inaccuracy will become serious. In order to overcome this difficulty, recall that the map:

$$(e_1, e_2) \to e_1 \wedge e_2$$

is *bilinear*, i.e., linear in *each* argument, and rewrite (3.6) as

$$\frac{1}{T}\ln\frac{\|[(D\varphi^T)_{x_0} \wedge (D\varphi^T)_{x_0}](e_1 \wedge e_2)\|}{\|e_1 \wedge e_2\|} \tag{3.7}$$

where

$$(D\varphi^T)_{x_0} \wedge (D\varphi^T)_{x_0} \tag{3.8}$$

is the induced linear map [13]. Since this is a 3×3 matrix and since

$$e_{12} \triangleq e_1 \wedge e_2 \tag{3.9}$$

is a 3-dimensional vector, we can compute (3.5) without the above difficulty. The initial vector e_{12} of (3.9) can be chosen *arbitrarily* for the same reason that e of (3.4) can be chosen arbitrarily, provided that $\mu_1(x_0)+\mu_2(x_2)$ dominates $\mu_1(x_0)+\mu_3(x_0)$ and $\mu_2(x_0)+\mu_3(x_0)$ by reasonable margins.

Finally, there is also some difficulty in computing $\mu_3(x_0)$ alone for the same reason as before. We compute, instead,

$$\mu_1(x_0)+\mu_2(x_0)+\mu_3(x_0) \tag{3.10}$$

which gives the average contraction or expansion rate of a *volume element* in $E^1_{x_0}$ assuming that $E^1_{x_0} = T_{x_0}\mathbb{R}^3$. An argument similar to the above shows that

$$\frac{1}{T}\ln\frac{\|[(D\varphi^T)_{x_0} \wedge (D\varphi^T)_{x_0} \wedge (D\varphi^T)_{x_0}](e_1 \wedge e_2 \wedge e_3)\|}{\|e_1 \wedge e_2 \wedge e_3\|} \tag{3.11}$$

would eventually give (3.10), where

$$\operatorname{span}\{e_1, e_2, e_3\} = E^1_{x_0} = T_{x_0}\mathbb{R}^3.$$

3.2. Computations

Based on the above algorithms, we computed the Lyapunov exponent $\mu_1(x_0)$ by solving the variation equation

$$\frac{dy}{dt} = (DF)_{\varphi^t(x_0)}y \tag{3.12}$$

with

$$y(0) = e, \qquad \|e\| = 1$$

and then computing

$$\frac{1}{T}\ln\|y(T)\|. \tag{3.13}$$

Our computation gives

$$\mu_1(x_0) \approx 0.23 \tag{3.14}$$

where

$$\begin{cases} x_0 = (-1.7713, 0.0527854, 1.74606) \\ e = \left(\frac{1}{\sqrt{3}}, \frac{1}{\sqrt{3}}, \frac{1}{\sqrt{3}}\right) \\ T = 3000. \end{cases} \tag{3.15}$$

Of course, one has to periodically renormalize $y(t)$ after a reasonable amount of time since $\|y(t)\|$ gets very large. More specifically, letting $T = n\tau$, one sees that

$$\begin{aligned} &\frac{1}{T}\ln\|y(T)\| \\ &= \frac{1}{n\tau}\ln\|(D\varphi^{n\tau})y(0)\| \\ &= \frac{1}{n\tau}\ln(\|(D\varphi^\tau)_{x((n-1)\tau)}y((n-1)\tau)\|/\|y(0)\|) \\ &= \frac{1}{n\tau}\ln\left(\frac{\|(D\varphi^\tau)_{x((n-1)\tau)}y((n-1)\tau)\|}{\|(D\varphi^\tau)_{x((n-2)\tau)}y((n-2)\tau)\|} \cdot \frac{\|(D\varphi^\tau)_{x((n-2)\tau)}y((n-2)\tau)\|}{\|(D\varphi^\tau)_{x((n-3)\tau)}y((n-3)\tau)\|} \cdots \frac{\|(D\varphi^\tau)_{x_0}y(0)\|}{\|y(0)\|}\right) \\ &= \frac{1}{n\tau}\sum_{k=0}^{n-1}\ln\frac{\|(D\varphi^\tau)_{x(k\tau)}y(k\tau)\|}{\|y(k\tau)\|}. \end{aligned} \tag{3.16}$$

If one renormalizes

$$\| y(k\tau) \| = 1$$

at each k, then

$$\frac{1}{T}\ln\| y(T)\| = \frac{1}{n\tau}\sum_{k=0}^{n-1}\ln\|(D\varphi^{\tau})_{x(k\tau)}y(k\tau)\|. \quad (3.17)$$

In our case, we chose $\tau = 10$ with a Runge–Kutta step size equal to 0.005. Our experience indicates that (3.14) is insensitive to the initial tangent vector e and to the initial condition x_0. The time $T = 3000$ seems to be enough for convergence.

In order to compute (3.7) let

$$y \triangleq (D\varphi^{t})_{x_0}e_1,\ z \triangleq (D\varphi^{t})_{x_0}e_2.$$

Then

$$\begin{aligned}\frac{d}{dt}(y \wedge z) &= \frac{dy}{dt}\wedge z + y \wedge \frac{dz}{dt}\\ &= \left[(DF)_{\varphi^{t}(x_0)}y\right]\wedge z + y\wedge\left[(DF)_{\varphi^{t}(x_0)}z\right]\\ &= \left[(DF)_{\varphi^{t}(x_0)}\wedge \mathbf{1} + \mathbf{1}\wedge(DF)_{\varphi^{t}(x_0)}\right] y\wedge z\end{aligned} \quad (3.18)$$

where $\mathbf{1}$ is the 3×3 identity matrix and

$$\left[(DF)_{\varphi^{t}(x_0)}\wedge\mathbf{1}\right](e_i\wedge e_j) \triangleq \left((DF)_{\varphi^{t}(x_0)}e_i\right)\wedge e_j$$

$$\left[\mathbf{1}\wedge(DF)_{\varphi^{t}(x_0)}\right](e_i\wedge e_j) \triangleq e_i\wedge\left((DF)_{\varphi^{t}(x_0)}e_j\right).$$

(An explicit formula is given in the Appendix). Therefore, solving the "2-dimensional" variational equation (3.18) with

$$\|(y\wedge z)(0)\| = \|e_{12}\| = 1$$

one can compute

$$\frac{1}{T}\ln\|(y\wedge z)(T)\|.$$

Our computation gives

$$\mu_1(x_0) + \mu_2(x_0) \approx 0.23 \quad (3.19)$$

where x_0 and T are the same as before and

$$e_{12} = \left(\frac{1}{\sqrt{3}}, \frac{1}{\sqrt{3}}, \frac{1}{\sqrt{3}}\right).$$

Again (3.19) appears to depend on neither x_0 nor e_{12}.

Finally, observing that

$$(D\varphi^{t})_{x_0}\wedge(D\varphi^{t})_{x_0}\wedge(D\varphi^{t})_{x_0} = \det(D\varphi^{t})_{x_0} \quad (3.20)$$

and

$$\frac{d}{dt}\det(D\varphi^{t})_{x_0} = \mathrm{trace}(DF)_{\varphi^{t}(x_0)}\det(D\varphi^{t})_{x_0} \quad (3.21)$$

one can compute (3.11). Our computation with the same x_0 and T gives

$$\mu_1(x_0) + \mu_2(x_0) + \mu_3(x_0) \approx -1.55. \quad (3.22)$$

It follows from (3.14), (3.19), and (3.22) that

$$\begin{cases}\mu_1(x_0) \approx 0.23\\ \mu_2(x_0) \approx 0\\ \mu_3(x_0) \approx -1.78.\end{cases} \quad (3.23)$$

This shows that in the double-scroll attractor observed, certain line elements are expanded, area elements are preserved and volume elements are contracted. This agrees with the sheet-like structure described in Section II. It would be interesting to compare (3.23) with those of the Lorenz attractor. Even though the parameter values in [14] are different ($\sigma = 16$, $\beta = 4$, $\rho = 40$) from the popular ones, they are enough for our present purpose:

$$\begin{cases}\mu_1(x_0) \approx 1.37\\ \mu_2(x_0) \approx 0\\ \mu_3(x_0) \approx -22.37.\end{cases} \quad (3.24)$$

The Lorenz attractor has much sharper expansion and contraction rates than the double-scroll attractor. Note also that in the Lorenz attractor, volume elements are contracted uniformly since its divergence = constant = -21.

3.3. Lyapunov Dimension

Dimension of a chaotic attractor is one of the very few quantitative measures which are associated with chaotic attractors. Among the various different definitions of dimension of chaotic attractors [15] we compute the *Lyapunov dimension* since it naturally comes from Lyapunov exponents. We do not claim that this is the most appropriate one. Recall (3.23) and recall that our numerical results indicate that these numbers do not seem to depend on x_0. *Assume* that this is, in fact, the case. Then, since μ_1, $\mu_1 + \mu_2 > 0$ and since $\mu_1 + \mu_2 + \mu_3 < 0$, the Lyapunov dimension is given by [15]

$$d_L = 2 + \frac{\mu_1 + \mu_2}{|\mu_3|} \approx 2.13 \quad (3.25)$$

Let us compare this number with the Lorenz attractor. It follows from (3.24) that for the Lorenz attractor,

$$d_L = 2 + \frac{1.37}{22.37} \approx 2.06. \quad (3.26)$$

Both of them are *fractals* between 2 and 3 which agree with the sheet-like structure observed. Since (3.25) is greater than (3.26), one might say that our attractor is slightly "thicker" than the Lorenz attractor (with $\sigma = 16$, $\beta = 4$, $\rho = 40$).

IV. Power Spectra

Fig. 16 shows the power spectra for the time waveforms of the three state variables. In each case $N = 2^{16}$ Runge–Kutta iterations were performed with a step size equal to 0.04.[10] The figures show the components of the first $M = N/2^4 = 2^{12}$ normalized frequencies in log–log scale. The vertical scale is 10 dB/division. In each case, there is a sharp peak at $f = 828$ (identified by the vertical arrow). This roughly corresponds to the oscillatory component $j\omega_p$ of the complex-conjugate eigenvalue $\sigma_P \pm j\omega_P$ at $P^{\pm}$. Indeed, one has $2\pi/(N\times 0.04/828) \approx 1.99$ and it roughly checks with $\omega_P \approx 2.13$ (Recall Section I). Note also

[10] It is well known that FFT is very efficient if the number of samples is a power of 2.

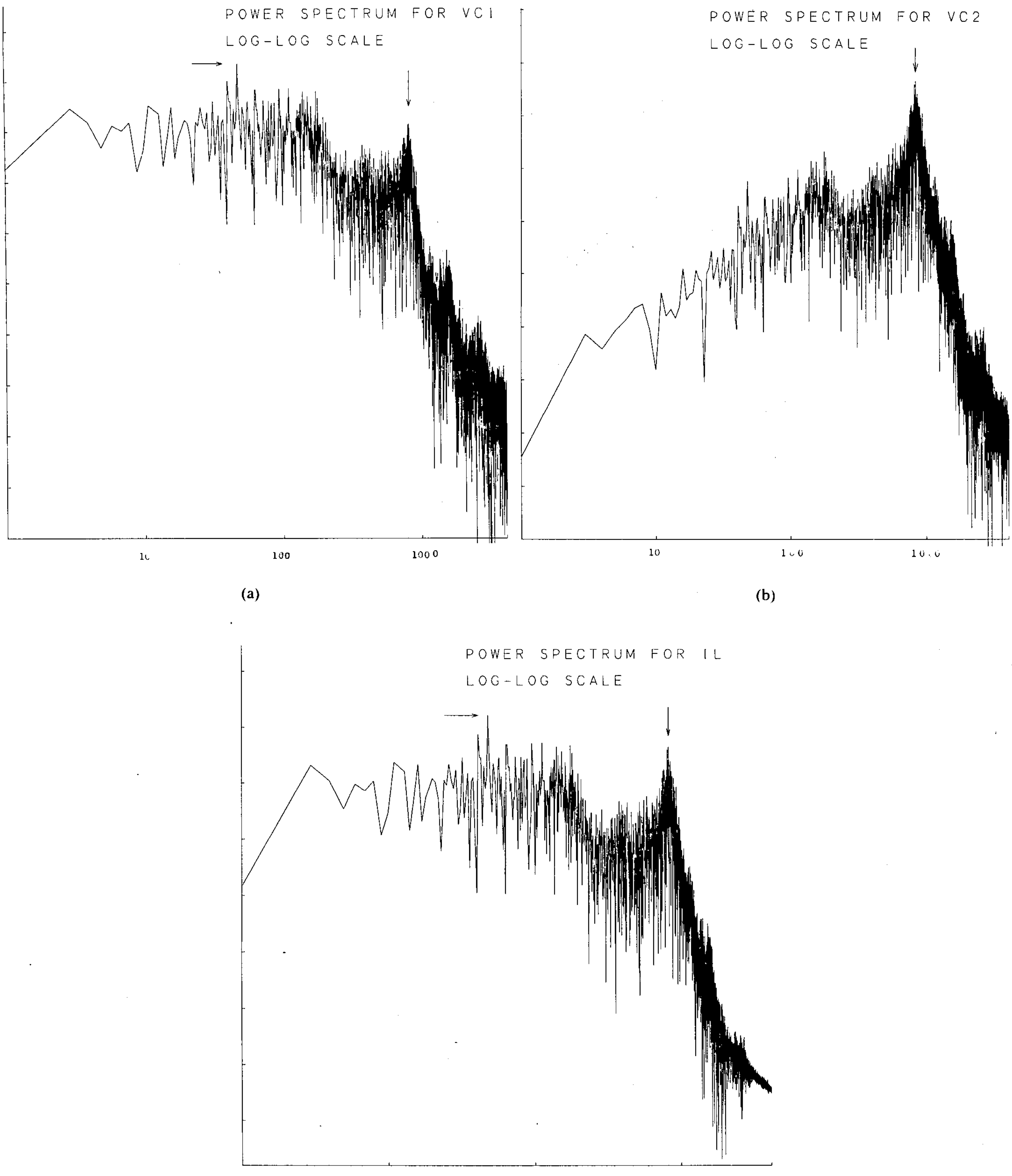

Fig. 16. Power spectra of time waveforms associated with the three state variables: (a) v_{C_1}. (b) v_{C_2}. (c) i_L. Vertical scale: 10 dB/division. Horizontal axis: normalized frequency.

that $N \times 0.04/828 \approx 3.166$ roughly corresponds to the time a typical trajectory takes in rotating around $\boldsymbol{P}^+$ or $\boldsymbol{P}^-$. The power spectra for v_{C_1} and i_L have notable lower frequency components while the power spectrum for v_{C_2} does not have such lower frequency components. This stems from the fact that the v_{C_2}-component of $\boldsymbol{P}^+$ and $\boldsymbol{P}^-$ is zero while the v_{C_1}-component and the i_L-component are nonzero, and therefore, the oscillations of v_{C_2} have essentially no "dc" bias while the oscillations of v_{C_1} and i_L are biased. The peak in the lower frequency components is at $f = 48$ (identified by the horizontal arrow) which corresponds to the fact that the trajectory has gone "up and down" for 48 times, i.e., it has traversed the process $D_1 \to D_0 \to D_{-1}$ (see Section II) for 48 times and $D_{-1} \to D_0 \to D_1$ for another 48 times.

Fig. 17 shows power spectra for v_{C_1} and v_{C_2} measured from the circuit of Fig. 4. The correspondence with the digital computations is clear.

V. Concluding Remarks

1) One of the reviewers pointed out that Shilnikov's theorem [4, section 6.5] might be applicable[11] to our equation (1.1). Indeed we have already observed orbits near homoclinicity experimentally and numerically. The result will be reported elsewhere, however.

2) Another reviewer brought our attention to Glendinning's work [16], where third order systems with symmetry are discussed. The example system of [16] has, for certain parameter ranges, equilibria with the same stability types as our circuit, and chaotic attractors have been observed among other phenomena, even though the system is not piecewise linear.

3) We are grateful to another reviewer who called our attention to a more recent paper [17] which contains power spectra associated with the system discussed in [10]. The relationship, if there is any, between those power spectra in [17] and Figs. 16 and 17 of the present paper is not clear, however.

Appendix

Here we will give an explicit formula for (3.18). Let $\{\boldsymbol{e}_1, \boldsymbol{e}_2, \boldsymbol{e}_3\}$ be the standard basis for $\mathbb{R}^3$. Then $\boldsymbol{e}_1 \wedge \boldsymbol{e}_2 = \boldsymbol{e}_{12}$, $\boldsymbol{e}_2 \wedge \boldsymbol{e}_3 = \boldsymbol{e}_{23}$, $\boldsymbol{e}_1 \wedge \boldsymbol{e}_3 = \boldsymbol{e}_{13}$ are the standard basis for $(\mathbb{R}^3_2)^*$, the set of all alternating bilinear functions on $\mathbb{R}^3 \times \mathbb{R}^3$ [13] where $\wedge$ denotes the exterior product. They satisfy,

$$\boldsymbol{e}_i \wedge \boldsymbol{e}_j = -\boldsymbol{e}_j \wedge \boldsymbol{e}_i, \qquad \boldsymbol{e}_i \wedge \boldsymbol{e}_i = \boldsymbol{0}.$$

Since (see (1.1))

$$(\boldsymbol{DF})_x = \begin{bmatrix} -\frac{1}{C_1}(G + (Dg)_{v_{C_1}}) & \frac{1}{C_1}G & 0 \\ \frac{1}{C_2}G & -\frac{1}{C_2}G & \frac{1}{C_2} \\ 0 & -\frac{1}{L} & 0 \end{bmatrix}$$

one can easily compute

$$(\boldsymbol{DF})_x \wedge \boldsymbol{1} = \begin{bmatrix} -\frac{1}{C_1}(G + (Dg)_{v_{C_1}}) & 0 & 0 \\ 0 & -\frac{1}{C_2}G & \frac{1}{C_2}G \\ 0 & \frac{1}{C_1}G & -\frac{1}{C_1}(G + (Dg)_{v_{C_1}}) \end{bmatrix}$$

$$\boldsymbol{1} \wedge (\boldsymbol{DF})_x = \begin{bmatrix} -\frac{1}{C_2}G & 0 & \frac{1}{C_2} \\ 0 & 0 & 0 \\ -\frac{1}{L} & 0 & 0 \end{bmatrix}.$$

Therefore,

$$(\boldsymbol{DF})_x \wedge \boldsymbol{1} + \boldsymbol{1} \wedge (\boldsymbol{DF})_x = \begin{bmatrix} -\left(G\left(\frac{1}{C_1} + \frac{1}{C_2}\right) + \frac{1}{C_1}(Dg)_{v_{C_1}}\right) & 0 & \frac{1}{C_2} \\ 0 & -\frac{1}{C_2}G & \frac{1}{C_2}G \\ -\frac{1}{L} & \frac{1}{C_1}G & -\frac{1}{C_1}(G + (Dg)_{v_{C_1}}) \end{bmatrix}.$$

Remark: Theoretically, there is some difficulty in using (3.12), (3.18), and (3.21) because $g(\cdot)$ is piecewise-linear and Dg has discontinuities at $v_{C_1} = \pm 1$. Numerically, however, there seem to be no problem if one chooses a small enough Runge–Kutta step size.

[11] It asserts, in the present context, that if there is a homoclinic trajectory at the origin, and if $\gamma_0 > |\sigma_0|$, i.e., the real eigenvalue is greater than the magnitude of the real part of the complex eigenvalues, then there exist a countably many saddle-type closed orbits in an arbitrary neighborhood of the homoclinic orbit.

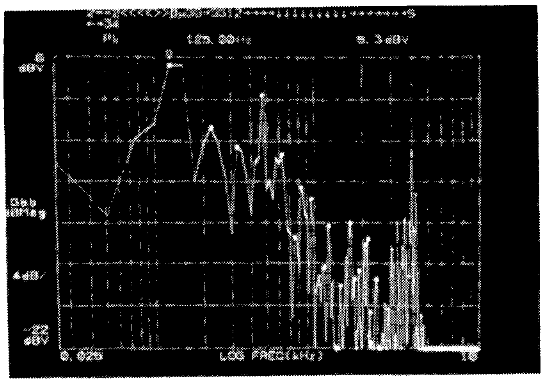

(a)

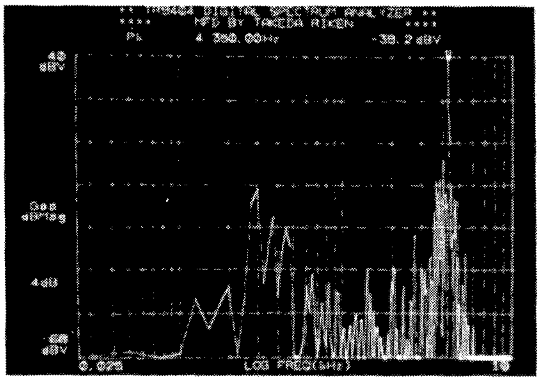

(b)

Fig. 17. Power spectra measured from the circuit of Fig. 4: (a) v_{C_1}. (b) v_{C_2}.

Acknowledgment

During the course of this work, the authors have had exciting discussions with their friends, G. Ikegami of Nagoya University, S. Ichiraku of Yokohama City University, M. Ochiai of Shohoku Institute of Technology, Y. Togawa of Science University of Tokyo, K. Sawata of Toyohashi University of Technology and Science, S. Tanaka, T. Ando, H. Tomonaga, R. Tokunaga, J. Sato and K. Tokumasu of Waseda University. The authors are indebted to I. Shimada for discussions on Lyapunov exponents. They also thank all the reviewers for many valuable comments and suggestions.

References

[1] T. Matsumoto, "A chaotic attractor from Chua's circuit," *IEEE Trans. CAS*, vol. CAS-31, pp. 1055–1058, Dec. 1984.

[2] G-Q. Zhong and F. Ayrom, "Experimental confirmation of chaos from Chua's circuit," *Int. J. Circuit Theory Appl.*, vol. 13, pp. 93–98, Jan. 1985.

[3] L. O. Chua and S. M. Kang, "Section-wise piecewise-linear functions: canonical representation, properties, and applications," *Proc. IEEE, vol.* 65, *pp.* 915–929, *June* 1977.

[4] J. Guckenheimer and P. Holmes, *Nonlinear Oscillations, Dynamical Systems, and Bifurcations of Vector Fields*. New York: Springer, 1983.

[5] L. O. Chua and P. M. Lin, *Computer Aided Analysis of Electronic Circuits: Algorithms and Computational Techniques*. Englewood Cliffs, NJ: Prentice-Hall, 1975.

[6] M. W. Hirsch and S. Smale, *Differential Equations, Dynamical Systems, and Linear Algebra*. New York: Academic, 1974.

[7] E. Lorenz, "Deterministic non-periodic flows," *J. Atmos. Sci.*, vol. 20, pp. 130–141, 1963.

[8] O. Rössler, "An equation for continuous chaos," *Phys. Lett.*, vol. 57A, pp. 397–398, 1976.

[9] C. T. Sparrow, "Chaos in a three dimensional single loop feed back system with a piecewise linear feedback function," *J. Math. Anal. Appl.*, vol. 83, pp. 275–291, 1981.

[10] R. W. Brockett, "On conditions leading to chaos in feedback systems," in *Proc. 1982 CDC*, Dec. 1982.

[11] L. O. Chua, "Dynamic nonlinear networks: state of the art," *IEEE Trans. Circuits Syst.*, vol. CAS-27, pp. 1059–1087, Nov. 1980.

[12] V. I. Oseledec, "A multiplicative ergodic theorem: Lyapunov characteristic numbers for dynamical systems," *Trans. Moscow Math. Soc.*, vol. 19, pp. 197–231, 1968.

[13] W. H. Fleming, *Functions of Several Variables*. Reading, MA: Addison-Wesley, 1965.

[14] I. Shimada and T. Nagashima, "A numerical approach to ergodic problem of dissipative dynamical systems," *Progr. Theor. Phys.*, vol. 61, pp. 1605–1616, 1979.

[15] L. S. Young, "Entropy, Lyapunov exponents and Hausdorff dimension in differentiable dynamical systems," *IEEE Trans. Circuits Syst.*, vol. CAS-30, pp. 599–607, 1983.

[16] P. Glendinning, "Bifurcations near homoclinic orbits with symmetry," *Phys. Lett.*, vol. 103 A, pp. 163–166, 1984.

[17] R. W. Brockett and J. Loncaric, "Chaos and randomness in dynamical system," in *Proc. 1983 CDC*, Dec. 1983.

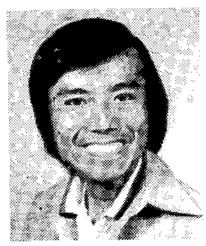

Takashi Matsumoto (M'71–F'85) was born in Tokyo, Japan, on March 30, 1944. He received the B. Eng. degree in electrical engineering from Waseda University, Tokyo, Japan, the M.S. degree in applied mathematics from Harvard University, Cambridge, MA, and the Dr. Eng. degree in electrical engineering from Waseda University, Tokyo, in 1966, 1970, and 1973, respectively.

Presently he is Professor of Electrical Engineering, Waseda University, Tokyo, Japan. From 1977 to 1979, he was on leave with the Department of Electrical Engineering and Computer Sciences, University of California, Berkeley, CA. His interest is in nonlinear networks. He was an Overseas Associate Editor of the IEEE TRANSACTIONS ON CIRCUITS AND SYSTEMS.

Leon O. Chua (S'60–M'62–SM'70–F'74) was born in the Philippines on June 28, 1936, of Chinese nationality. He received the B.S.E.E. degree from Mapua Institute of Technology, Manila, the Philippines, in 1959, the S.M. degree from Massachusetts Institute of Technology, Cambridge, in 1961, and the Ph.D. degree from the University of Illinois, Urbana, in 1964.

He worked for the IBM Corporation, Poughkeepsie, NY, from 1961 to 1962. He joined the Department of Electrical Engineering, Purdue University, Lafayette, IN, in 1964, as an Assistant Professor. Subsequently, he was promoted to Associate Professor in 1967, and to Professor in 1971. Immediately following this, he joined the Department of Electrical Engineering and Computer Sciences, University of California, Berkeley, where he is currently Professor of Electrical Engineering and Computer Sciences. His research interests are in the areas of general nonlinear network and system theory. he has been a consultant to various electronic industries in the areas of nonlinear network analysis, modeling, and computer-aided design. He is the author of *Introduction to Nonlinear Network Theory* (New York: McGraw-Hill, 1969) and coauthor of the book *Computer-Aided Analysis of Electronic Circuits: Algorithms and Computational Techniques* (Englewood Cliffs, NJ: Prentice-Hall, 1975). He has also published many research papers in the area of nonlinear networks and systems. He was the Guest Editor of the November 1971. Special Issue of IEEE TRANSACTIONS ON EDUCATION on "Applications of Computers to Electrical Engineering Education," the Editor of the IEEE TRANSACTIONS ON CIRCUITS AND SYSTEMS from 1973 to 1975, and the Guest Editor of the August and September special issues of the IEEE TRANSACTIONS ON CIRCUITS AND SYSTEMS on "Nonlinear Phenomena, Modeling, and Mathematics." Dr. Chua is presently a Deputy Editor of the International Journal of Circuit Theory and Applications.

Dr. Chua is a member of Eta Kappa Nu, Tau Beta Pi, and Sigma Xi. He was a member of the Administrative Committee of the IEEE Circuits and Systems Society from 1971 to 1974, and the past President of the IEEE Circuits and Systems Society. He has been awarded four patents and is a recipient of the 1967 IEEE Browder J. Thompson Memorial Prize Award, the 1973 IEEE W. R. G. Baker Prize Award, the 1973 Best Paper Award of the IEEE Circuits and Systems Society, the Outstanding Paper Award at the 1974 Asilomar Conference on Circuits, Systems, and Computers, the 1974 Frederick Emmons Terman Award, the 1976 Miller Research Professorship from the Miller Institute, the 1982 Senior Visiting Fellowship at Cambridge University, England, the 1982–1983 Alexander Humboldt Senior U.S. Scientist Award at the Technical University of Munich, W. Germany, and the 1983–1984 visiting U.S. Scientist Award at Waseda University, Tokyo, from the Japan Society for Promotion of Science. In May 1983, he received an Honorary Doctorate (Doctor honoris causa) from the Ecole Polytechnique, Federal de Lausanne, Switzerland. In July 1983, Dr. Chua was awarded an Honorary Professorship at the Chengdu Institute of Radio Engineering in Sichuan, the Peoples Republic of China. In 1984, he was awarded an Honorary Doctorate at the University of Tokushima, Japan, and the IEEE Centennial Medal. In 1985, Dr. Chua was awarded the Waseda University International Fellowship from Japan, and the IEEE Guillemin-Cauer Prize for the best paper published in 1984–1985.

Motomasa Komuro was born in Tokyo, Japan, on December 15, 1954. He received the B.S. degree in 1979, the M.S. degree in 1981, and the Ph.D. degree in 1985, all in mathematics from Tokyo Metropolitan University, Tokyo, Japan.

His main research area is the theoretical study of dynamical systems.

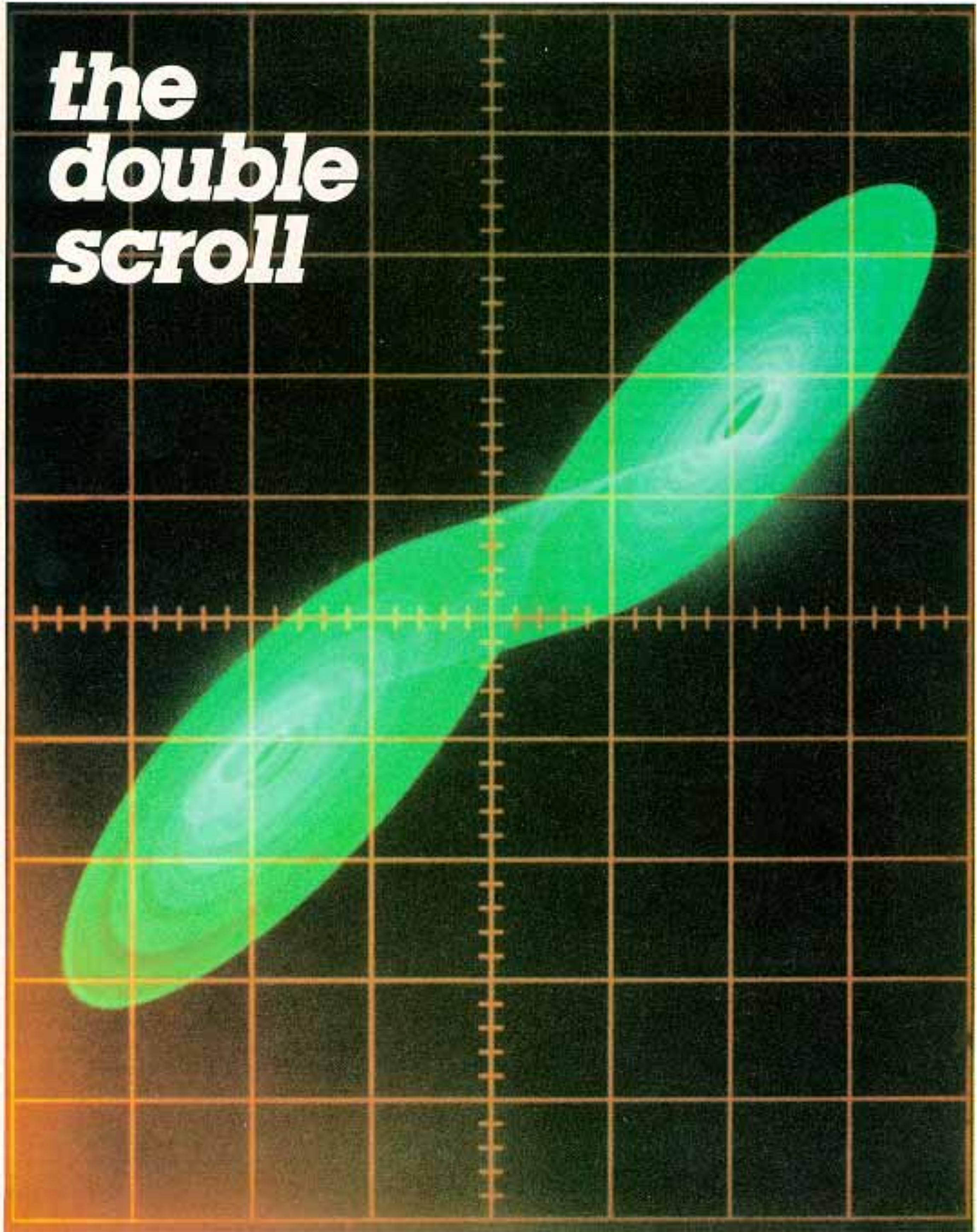
the double scroll